博士学位論文

Study on the post-2015 absence of Chandler wobble: Calculation of the excitation function based on JRA-55 and OFES2

（2015年のチャンドラー極運動の消失:

JRA-55及びOFES2に基づいた励起関数の計算）

山口　竜史

北海道大学大学院理学院　自然史科学専攻

令和8年3月

INDEX

ABSTRACT

The Chandler wobble is one component of the Earth's polar motion and is considered to correspond to the free oscillation of the solid Earth. We have found that the Chandler wobble was absent from 2015 to 2021 for the first time in the observational history. Although it is recognised that the excitation sources of the Chandler wobble are the atmosphere, ocean, and land water, the precise excitation mechanism, Chandler period, and the quality factor are still open questions.

In this study, to investigate the cause of the absence of the Chandler wobble and clarify its excitation mechanism, excitation functions were calculated based on atmospheric reanalysis data JRA-55 and ocean model OFES2 data. Furthermore, we integrated the three atmospheric angular momentum including the one based on the JRA-55, two oceanic angular momentum, and one hydrospheric angular momentum to determine their respective contributions to the excitation of the Chandler wobble. The results revealed that the atmospheric contribution including the one estimated from the JRA-55, decreased around the same time as the absence of the Chandler wobble. This result suggests that changes in atmospheric behaviour can be involved in the absence. On the other hand, the contribution from the ocean was found to be inconsistent across the model datasets used, indicating that new data will be required to estimate the oceanic contribution more accurately.

The oceanic angular momentum derived from the OFES2 ocean model was calculated. As a result, it showed a little discrepancy from existing estimates in the velocity term associated with ocean currents. However, the matter term, which reflects the redistribution of the seawater, exhibited an amplitude approximately twice as large as that in other data. For validation, ocean bottom pressure computed from the OFES2 model was compared with that from the ECCO ocean model. The results showed that the two results are strongly correlated overall, whereas weak or even negative correlations were found elsewhere. One possible reason for this discrepancy is that the OFES2 ocean model is not

assimilated with observational data, indicating that some form of correction will be required to improve its accuracy.

The quality factor, Q, is a constant on the damping that has not been estimated with high precision. We investigated whether it can be inferred solely from observations of polar motion by taking advantage of the absence of the Chandler wobble. Assuming the Chandler period and Q value, we performed a deconvolution on the polar motion data to compute the excitation function, and next reintegrated it under the same assumption for comparison with the original observed data to attempt to estimate the Chandler period and Q. The results showed that the residuals between the two did not exceed the estimation error of the annual component, and no significant differences were identified. This result suggests that accurate estimation of the Chandler period and Q requires geophysical data.

In summary, this study computed and analysed new estimates of atmospheric, oceanic angular momentum in order to reveal the excitation and damping mechanisms of the Chandler wobble. In addition, we evaluated a method for estimating the Q value. These results provide new insights into long-standing problems on the Chandler wobble, including ones previously considered to have been resolved.

SUMMARY OF EACH CHAPTER

Chapter I reviews the current state of knowledge regarding the Chandler wobble and explains the absence of the Chandler wobble from 2015 previously examined in the master's thesis of the author.

Chapter II describes the calculation of a new atmospheric angular momentum data based on the JRA-55 reanalysis data, undertaken to analyse the atmospheric contribution to the excitation of the Chandler wobble, and examines the contribution of each component using this result together with available excitation function data.

Chapter III presents the calculation of oceanic angular momentum based on newly acquired ocean datasets, which is found through the analysis in Chapter II as well as its validation.

Chapter IV evaluates a method for estimating the Chandler period and the quality factor, *Q*, from only observed polar motion data, taking advantage of the absence of the Chandler wobble from 2015, and discusses the results.

Chapter V provides an overall conclusion of this thesis.

要旨

チャンドラー極運動は地球の極運動の 1 成分であり、固体地球の自由振動に相当する成分であると考えられている。我々はチャンドラー極運動が 2015 年から 2021 年の期間に、観測史上初めて消失していることを発見した。チャンドラー極運動の励起源は大気・海洋・陸水であるということが明らかになっているが、励起メカニズムや減衰に関する定数 Q 値はこれまで検討されてきたにもかかわらず、未だに励起メカニズムと Q については研究者による見解の違いがある。

本研究では、チャンドラー極運動消失の原因を探り、その励起メカニズムを明らかにするため、大気再解析データ JRA-55 に基づいて励起関数を計算した。さらに、JRA-55 に基づいて計算したものを含む NCEP・ECMWF・JRA-55 データに基づく大気角運動量、MPIOM・ECCO データに基づく海洋角運動量、LSDM データに基づく陸水角運動量を積分し、それぞれのチャンドラー極運動励起に対する寄与を求めた。その結果、JRA-55 による大気角運動量を含む大気の寄与について、チャンドラー極運動消失と同時期にその励起分が減少していることが明らかになった。この結果は、チャンドラー極運動の消失に大気の振る舞いの変化が関与していることを示唆している。一方、海洋の寄与については基づくモデルデータによって結果が整合的ではなく、海洋の寄与をより正確に見積もるには新たなデータが必要であることが分かった。

そこで、JRA-55 に基づいた風応力を駆動源とした海洋モデル OFES2 に基づいて海洋角運動量を計算した。その結果、海流による流速項は既存の海洋角運動量と大きな差異は無かったが、海水の質量再配分を反映する質量項では他の海洋角運動量のものの 2 倍程度の振幅を持っていた。検証のため、OFES2 海洋モデルから算出した海洋底圧力の値を ECCO 海洋モデルによるものと比較した。その結果、全体としては、両者は強く相関し OFES2 による海洋

底圧力の方がやや大きい値をとる傾向が見られた。一方で地域毎に比較すると、強い相関がみられる地域は低緯度或いは沿岸域に限られ、その他の地域では相関は弱いか負の相関があるということが明らかになった。この不整合の原因として考えられる一因は、OFES2 海洋モデルが観測データと同化されていないことが挙げられ、さらなる精度向上のためには何らかの補正が必要であると考えられる。

さらに、これまで精密に見積もられてこなかったチャンドラー極運動のクオリティーファクター(Q値)について、チャンドラー極運動消失を利用して、極運動の観測データのみで推定できるかを検証した。極運動データからチャンドラー周期及び Q 値を仮定して逆畳み込みを行って励起関数を計算し、これを同様の条件の下で再積分し元の観測データと比較することで、チャンドラー周期及びQ値の推定を試みた。その結果、両者の残差は年周成分の推定誤差を超えず、有意な差は見いだせないことが明らかになった。この結果は、チャンドラー周期及び Q 値の正確な推定には、地球物理学的データが必要となることを示唆している。

以上のように、本研究では、チャンドラー極運動の励起・減衰のメカニズムを明らかにするために、新たに大気角運動量及び海洋角運動量を計算し、他の角運動量データと比較し、それらの寄与を解析した。加えて、Q値の新たな推定手法に対して検証を行った。これらは長らく解決済みとされてきたものを含む、チャンドラー極運動に関する諸問題に対して、新たな知見を齎すものである。

各章の構成

第 I 章では、チャンドラー極運動に関するこれまでの知見と、修士論文で論じた、2015 年以降のチャンドラー極運動の消失について論じる。

第 II 章では、チャンドラー極運動励起に対する大気による寄与の解析のため、JRA-55 再解析データに基づく新たな大気角運動量の計算と、これを含めた既存の励起関数データに基づいた各成分による寄与の解析について述べる。

第 III 章では、第 II 章による解析によって必要とされた、新たな海洋データに基づく海洋角運動量の計算と、その検証について述べる。

第 IV 章では、2015 年以降のチャンドラー極運動の消失を利用した、極運動データのみに基づくチャンドラー周期及びクオリティーファクターの推定手法について検証し、その結果を論ずる。

第 V 章では本論文の内容を総観する。

I. INTRODUCTION

I.I. The Chandler Wobble

The Chandler wobble (CW) and annual wobble (AW) are two dominant near-circular components in the Earth's polar motion, a long-period (>1 day) motion of the Earth's spin axis relative to the rotating solid Earth (Munk and MacDonald 1960; Gross 2015). The AW is regarded as a "forced motion" by seasonal processes within fluids. On the other hand, the CW is thought of as a "free motion" of the solid Earth. The excitation source of the CW had been elusive until the 2000s (Gross 2015), and earthquakes were once examined as a candidate (e.g., Dahlen 1973). However, it is now widely accepted that the atmosphere, ocean, and continental water are the main sources (e.g., Furuya et al. 1996, 1997; Gross 2000; Aoyama et al. 2003; Nastula et al. 2007).

The period and the quality factor of the CW (P and Q, respectively) have been investigated by numerous studies. The estimated P, while having a certain range, is concentrated around 432 days. On the other hand, there are still a variety of estimated Q values ranging from 40 to 180 (e.g., Wilson and Vincente 1990; Furuya and Chao 1996; Seitz and Schmidt 2005; Seitz et al. 2012; Nastula and Gross 2015). These variations indicate that the excitation and damping mechanisms of the CW are still not perfectly understood.

Figure 1-1 shows the Earth orientation parameter (EOP) 20 C04 (IAU 2000A), which is the observed polar motion data provided by the International Earth Rotation and Reference Service (IERS) (Bizouard et al. 2019). The "IAU 2000A" stands for the version of the precession and nutation model used in deriving the polar motion data. In the data shown in Figure 1-1, the 6-year beat is caused by the AW and the CW. The beat had not been observed since 2015 and was approaching a sine curve with a one-year period, which implies the absence of the CW.

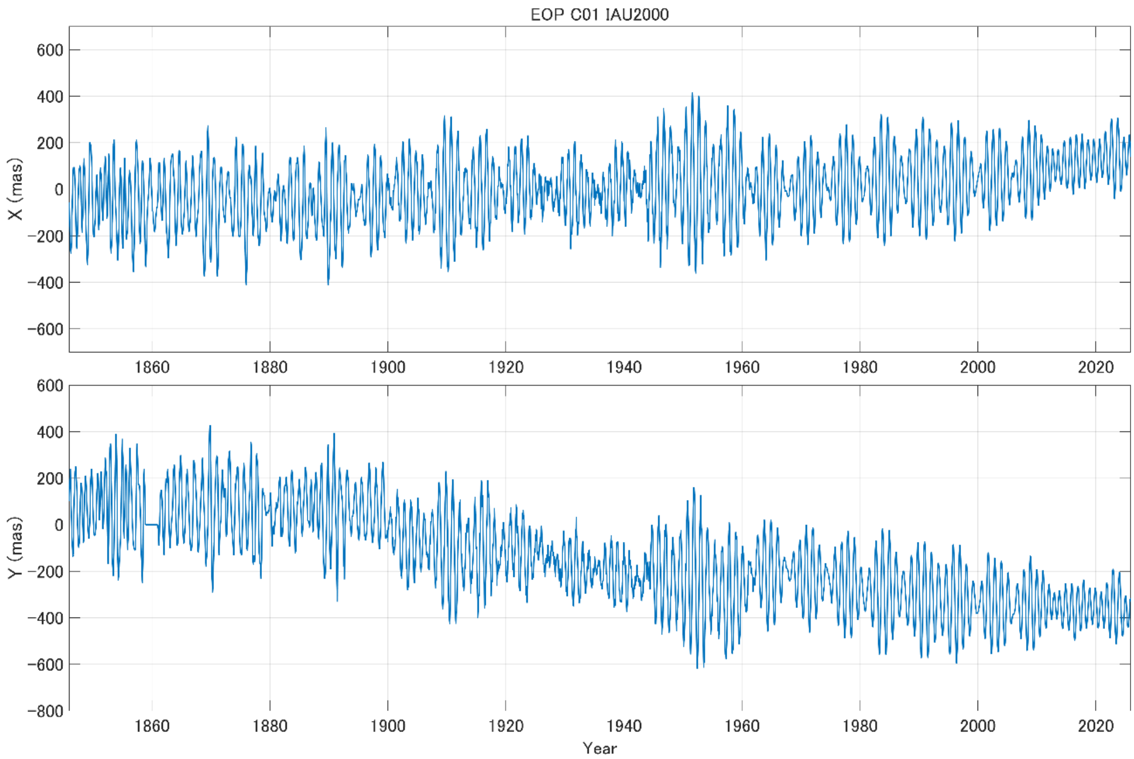

[Figure 1-1] Time series of the EOP C01 IAU2000 provided by the IERS.

I.II. Mechanism of the Excitation of the CW

[Table 1-1] The estimated *P* and *Q* by previous studies with data span and the reference source(s).

***P* (days)**	***Q***	**Span (yrs)**	**Reference (Source)**
435.2±2.6	**100 (50-400)**	70	Wilson and Haubrich (1976)
436.0±2.0	**96 (50-300)**	70	Ooe (1978), Complex ARMA
433.3±3.1	**179**	78	Wilson and Vicente (1990) (ML)
433.7±1.8	**49 (35, 100)**	10.8	Furuya and Chao (1996) (AAM)
432.98	**97**	60	Seitz et al. (2012) (AAM+OAM)

430.9±0.7	**127** (56, 255)	25	Nastula and Gross (2015) (AAM+OAM+HAM)
433.8±2.6	**39±18**	15	Ding and Chao (2017) (GPS U/D-displacement)

A number of studies have estimated the *P* and *Q* of the CW, the results of which are shown in Table 1-1. The estimated *P* values cluster around 432 days. On the other hand, there is a large variation in the estimated *Q* values from 39 to 179. It means our incomplete understanding of the excitation and damping processes. Precise estimation of *Q* allows for a more robust characterisation of the frequency-dependent deformation response of the solid Earth, particularly within the lower mantle (Smith and Dahlen, 1981), and aids in bridging the order-of-magnitude disparity observed across seismic, semi-diurnal, and long-period (18.6 years) frequency ranges (Benjamin et al. 2006).

The excitation source(s) of the CW have long remained uncertain, with earthquakes once considered a potential cause. However, it is now widely recognised that the atmosphere, ocean, and possibly continental water serve as its principal excitation sources. Despite this, it remains unresolved whether the excitation processes of the CW are random or resonant. Although some earlier studies conform to the near-resonant excitation model (e.g., Furuya et al. 1996, 1997; Aoyama et al. 2003), numerous previous studies on excitations of the CW have explicitly or implicitly assumed the Gaussian random process (e.g., Okubo 1982; Chao and Chung 2012).

Besides the geodynamical significant in the accurate estimates of *P* and *Q*. Prediction of the EOP plays important role in, for example, the positioning of the space craft and the enhancing the accuracy of the location on the Earth. In fact, the bulletin and prediction of the EOP is provided on the IERS website. Therefore, accurate estimates of the *P* and *Q* are crucial as they are essential for the physical prediction of EOP, which is socially needed.

I.III. Excitation mechanism of the CW

Excitation mechanism of the CW can be explained by the Liouville equation derived from the rotational equation of motion, $\frac{d\boldsymbol{H}}{dt} + \boldsymbol{\omega} \times \boldsymbol{H} = \boldsymbol{L}$ ($\boldsymbol{H}$, $\boldsymbol{\omega}$, and $\boldsymbol{L}$ are angular momentum, rotation vector, and external forces, respectively). The Liouville equation is:

$$\tilde{p} + \frac{i}{\tilde{\sigma}_{cw}} \frac{d\tilde{p}}{dt} = \tilde{\chi} \qquad (1-1)$$

where $\tilde{p}$ is the polar motion, $\tilde{\chi}$ is excitation function, and $\tilde{\sigma}_{cw}$ is the Chandler frequency:

$$\tilde{\sigma}_{cw} = \frac{2\pi}{P}\left(1 + \frac{i}{2Q}\right). \qquad (1-2)$$

The Q is the quality factor, which governs the strength of damping. The smaller Q implies stronger damping, whereas a larger Q implies weaker damping. The solution of Eq. (1-1) at t is

$$\tilde{p} = p(t_0)\exp[i\tilde{\sigma}_{CW}(t - t_0)] - i\tilde{\sigma}_{CW}\exp\,(i\tilde{\sigma}_{CW}t)\int_{t_0}^{t} \chi(\tau)\exp(-i\tilde{\sigma}_{CW}\tau)\,d\tau. \qquad (1-3)$$

The $\tilde{\chi}$ is excitation function, which consists of the atmospheric angular momentum (AAM), oceanic angular momentum (OAM), and hydrological angular momentum (HAM).

Figure 1-2 shows a conceptual figure of the second term of Eq. (1-3). Each plot of the power spectrum density represents the excitation function, the transfer function, and the polar motion, respectively. The AW and CW are interpreted as a convolution of the excitation function, which is the sum of the seasonal signals and white noise, and the transfer function of the Earth itself. Although the polar motion can be observed precisely thanks to the advance of the space geodesy, the excitation function and the transfer function remains uncertain. Moreover, while Figure 1-2 assumes “white noise” excitation, it is still an open question whether the CW excitation processes are random or resonant.

Although some earlier studies conform to the resonant excitation model (e.g., Furuya et al. 1996, 1997; Plag 1997; Aoyama and Naito 2001; Aoyama et al. 2003, Wang et al. 2025), numerous previous studies on excitations of the CW have explicitly or implicitly assumed the Gaussian random process (e.g., Okubo 1982; Chao and Chung 2012). To understand the excitation mechanism of the CW, it is necessary to accurately estimate the excitation function, or *P* and *Q*.

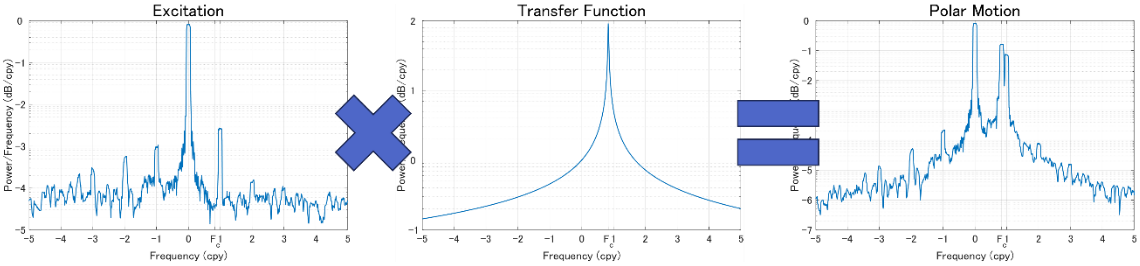

[Figure 1-2] A conceptual image of the excitation of the CW showing the excitation function (left), transfer function (middle), and the polar motion (right). The horizontal axis of each power spectrum density represents frequency (cycle per year), with clockwise rotation to the right of centre and counterclockwise rotation to the left.

Recently, long time-series excitation functions are limited two datasets: the combination of the AAM based on the NCEP/NCAR model and the OAM based on the ECCO v4r4 model provided by the Paris observatory (Salstein et al. 1993) and the combination of the AAM based on the ECMWF atmospheric model, the OAM based on the MPIOM ocean model, and HAM based on the LSDM model provided Deutsches GeoForschungs Zentrum (GFZ) (Dobslaw and Dill 2018). Recent studies on the CW have been relying solely on these datasets.

I.IV. Absence of the CW

As shown in Figure 1-1, we found that the 6-year beat, which was made by the AW and the CW, had become unclear. Taking advantage of it, we performed a simple least-squares modelling of the polar motion. The model consisting of the AW (prograde and retrograde), the CW, and the long-term motion is described as:

$$M(t) = A\exp\left(\frac{2\pi it}{365.25}\right) + B\exp\left(-\frac{2\pi it}{365.25}\right) + C\exp\left(\frac{2\pi it}{P}\right) + Dt^2 + Et + F. \qquad (1-4)$$

Therefore, the model without the CW after 2015 is described as:

$$M(t) = A\exp\left(\frac{2\pi it}{365.25}\right) + B\exp\left(-\frac{2\pi it}{365.25}\right) + Dt^2 + Et + F. \qquad (1-5)$$

We fit the model without the CW to the observed polar motion data after 2015 using the least square method (Figure 1-3a). The data we used is the EOP C04 (IAU 2000A) provided by IERS. Next, the CW was estimated by subtracting the modelled AW from the detrended polar motion data (Figure 1-3b). As a result, the amplitude of the CW became smaller than 30 milliarcseconds (mas), which means that the CW was absent from 2015 (Yamaguchi and Furuya 2024). We performed the same analysis for the extended time series back to 1890, using the polar motion data, EOP C01 IAU1980. The results confirmed the reduction in the CW amplitude in the 1920s, as reported by previous studies (e.g., Vondrák and Ron 2005; Malkin and Miller 2010), although an amplitude of about 100 mas remained. This indicates that the disappearance of the CW after 2015 is the first event in the observational history.

To examine the recent behaviour of the CW, the same analysis is conducted using the data available as of 2025. In this analysis, the fitting period of the AW is set from 2015 to 2019. The results shown in Figure 1-3b revealed that the CW amplitude began to increase around 2021, suggesting the reexcitation of the CW. However, it has not yet reached the amplitude as large as the one observed before its absence, indicating that a full recovery has not yet been achieved.

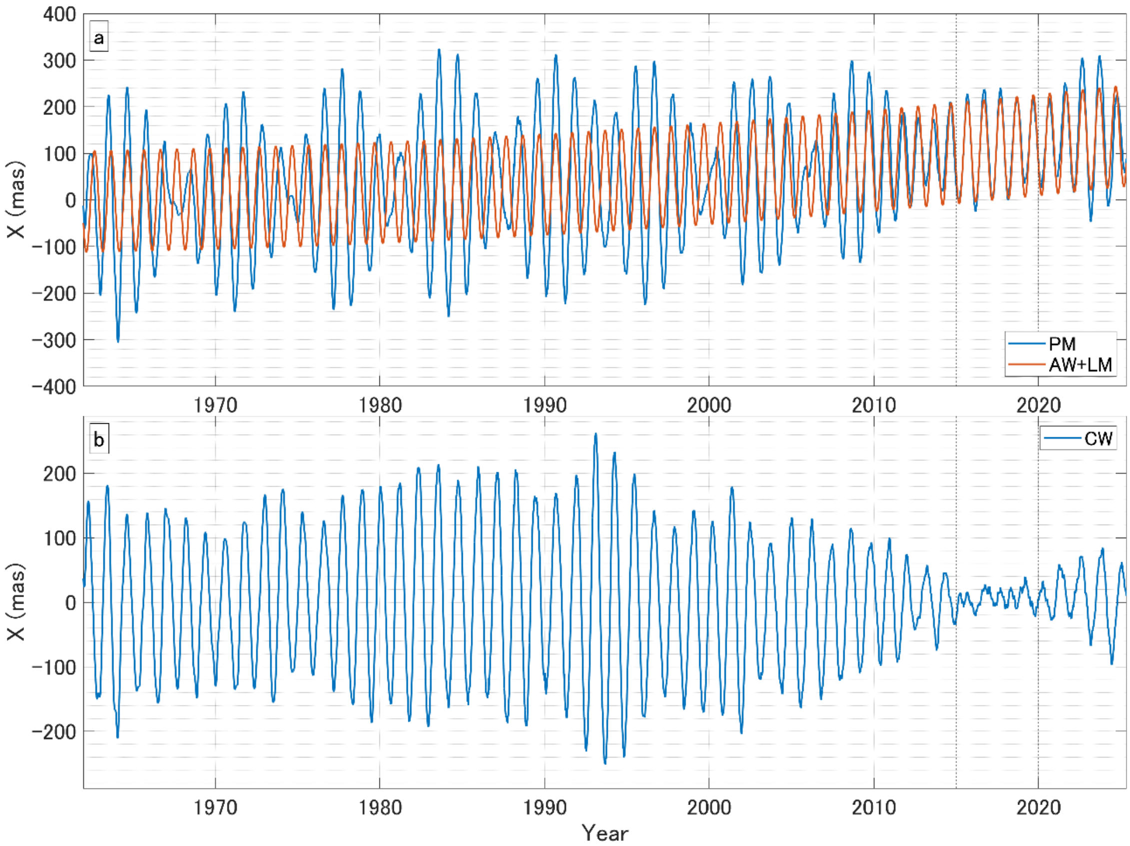

[Figure 1-3] (a) The observed polar motion data EOP 20 C04 provided by the IERS (blue) and the modelled AW and long-term motion (LM) using the least squares method (red). (b) The estimated CW is obtained by subtracting the AW + LM from the Polar motion (PM).

I.V. The atmospheric and oceanic data for polar motion

There are two combinations of the excitation function currently available, provided by Deutsches GeoForschungs Zentrum (GFZ) (Dobslaw and Dill 2017) and by the Atmospheric and Environmental

Research, Inc. and Jet Propulsion Laboratory (Salstein et al. 1993; Gross et al. 2003). In this study, new AAM and OAM are calculated based on the Japanese 55-year Reanalysis (JRA-55) (Kobayashi et al. 2015) and the Ocean General Circulation for the Earth Simulator version 2 (OFES2) (Sasaki et al. 2020), respectively.

JRA-55 data for the calculation of the AAM

The JRA-55 data, an atmospheric reanalysis provided by the Japan Meteorological Agency (JMA) (Kobayashi et al. 2015), is used to calculate the AAM. Since the observed data are reanalysed with a new and consistent model, the dataset remains temporally and spatially homogeneous and of high quality. The calculated AAM spans the period from 1960 to 2023, corresponding to the coverage of the dataset. The spatial grid resolution is 1.25 degrees horizontally, and the vertical levels consist of the surface and 60 isobars up to 0.1 hPa, allowing representation of phenomena in higher atmospheric layer. Although Furuya et al. (1996) and Aoyama and Naito (2001) emphasised the effect of wind excitation based on AAM derived from JMA objective analysis data, JMA AAM has not been used for studies on polar motion during the past two decades. In this study, the wind speed at each isobar and the ground surface and the surface pressure component are used to calculate the AAM.

[Table 1-2] Comparison of the atmospheric model used for the calculation of the AAM

	JRA-55 (Kobayashi et al. 2015)	**NCEP/NCAR (Kalnay et al. 1996)**	**ERA-Interim (Dee et al. 2011)**
Horizontal grid	~55 km	~210 km	~79 km

Vertical levels	Surface & 60 levels up to 0.1 hPa	28 levels up to 3 hPa	60 levels up to 0.1 hPa
Data assimilation method	4D-var	3D-var	4D-var

OFES2 data for the calculation of the OAM

The OFES2 is a quasi-global eddying ocean hindcast simulation developed by JAMSTEC (Sasaki et al. 2020). It has a high spatial resolution, with a 0.1-degree horizontal grid and 105 isobaric levels in the vertical, which enables representation of smaller-scale processes such as mesoscale eddies. Its resolution is higher than that of the ECCO model (1-degree grid and 50 isobars) and the MPIOM model used in Dobslaw and Dill (2017) (1-degree grid and 40 isobars). Yet, the true motivation to use OFES2 is not its high spatial-resolution but its atmospheric surface forcing is based on JRA-55. The JRA-55 is used as the atmospheric surface forcing, which enables to complement the JRA55 AAM.

Because of these features, the large-scale variability of sea surface height around the Gulf Stream, the Kuroshio, and the Antarctic Circumpolar Current agrees well with observations. On the other hand, some processes are not well simulated, such as the pathways of the Kuroshio and the Azores Current (Sasaki et al. 2020). We should note, however, that unlike ECCO data sets. OFES2 data is not assimilated with any observation data. Table 1-3 shows the comparison of the ocean models used for the calculation of the OAM.

[Table 1-3] The comparison of the oceanic models used for the calculation

	OFES2 **(Sasaki et al. 2020)**	**ECCO v4r4** **(Forget et al. 2015)**	**MPIOM** **(Jungclaus et al. 2013)**

Horizontal grid	0.1 degrees	1 degree	1 degree
Vertical levels	105	50	40
Data assimilation	No	Constrained	No

I.VI. The objective of this study

The clearly observed 6-year beat observed in the time-series of polar motion disappeared after 2015. A least-squares analysis revealed that the CW was absent after 2015 for the first time in the observational history. The objective of this study is to investigate the cause of this event and to use it as an opportunity to estimate the *P* and *Q*, which have not been accurately determined before, thereby providing further insight into the mechanism of the CW.

To explore the cause of the event, new AAM and OAM were calculated. These were analysed together with available AAM, OAM, and hydrospheric angular momentum (HAM) data to estimate the contributions of the atmosphere, ocean, and land water. We also examined if we could re-estimate the *P* and *Q*, taking advantage of the disappearance of the CW.

II. ATMOSPHERIC CONTRIBUTION TO THE ABSENCE OF THE CW

II.I. Introduction

The CW and AW are two dominant near-circular components in the Earth's polar motion, a long period (>1 day) motion of the Earth's spin axis relative to the rotating solid Earth (Munk and MacDonald 1960; Gross 2015). Because of their comparable amplitude and the 1.2-year period of the CW (P), the polar motion time series has been exhibiting a 6-year beat for over a century besides the secular drift of the mean pole toward the 79°W direction (Figures 2-1a). While the AW is a forced motion by seasonal angular momentum exchanges between surface fluids and the solid Earth around the equatorial axes, the CW, as a free oscillatory mode, requires one or more excitation sources that were elusive until the early 2000s (e.g., Gross 2015). While earthquakes were once considered as candidates but denied quantitatively (e.g., Dahlen 1973), it is now widely believed that the atmosphere, ocean, and possibly continental water are the excitation sources (e.g., Furuya et al. 1996; Aoyama and Naito 2001; Aoyama et al. 2003; Brzeziński and Nastula 2002; Gross 2000; Seitz and Schmidt 2005). However, there is still a threefold variation in the estimated Q of the CW from 50 to 179 that controls both its damping time and the required excitation power (e.g., Wilson and Vicente 1990; Furuya and Chao 1996; Seitz and Schmidt 2005; Seitz et al. 2012; Nastula and Gross 2015), indicating our incomplete understanding of the excitation sources and processes. Moreover, Q of the CW is a unique parameter that can constrain the frequency-dependent deformation response of the solid Earth, particularly the lower mantle (Smith and Dahlen 1981; Benjamin et al. 2006), and bridge the orders-of-magnitude gap between the seismic, semi-diurnal and long-period (18.6 years) tidal frequencies (Benjamin et al. 2006).

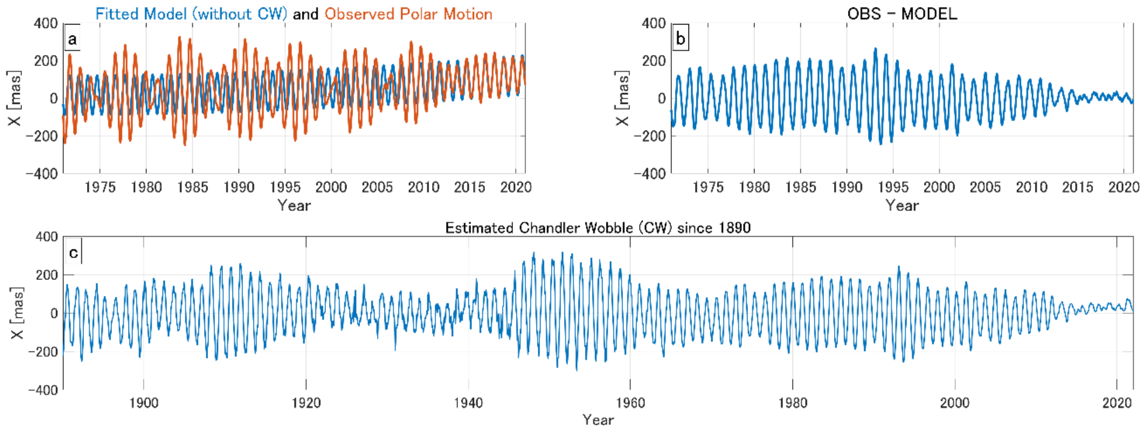

[Figure 2-1] The polar motion time-series. (a) The X-component of the polar motion data, EOP 14 C04, since 1976 (red) and the polar motion model (blue) by fitting the data from 2015 to 2021 with only the AW and long-term polar drift period and extending back to 1971. (b) Estimated CW since 1971 by taking a difference between the two time-series in (a). Note that we do not assume any Chandler period (*P*) and *Q* of the CW. (c) Similar to b but extended time-series back to 1890, using the polar motion data, EOP C01 IAU 1980.

Recent polar motion data lack the 6-year beat that was previously clearly observed (Figure 2-1a). While the CW amplitude is known to have been smallest in the 1920-40s (e.g., Vondrák and Ron 2005; Malkin and Miller 2010), we could readily recognize the presence of the 6-year beat even in the 1920-40s; we consider only the data after 1900 because the observation errors before 1900 are greater than 50 mas (International Earth Rotation and Reference System Service (IERS) website). The mas stands for milliarcsecond in angle, where one mas is equivalent to ~3 cm on the Earth surface. We show below by simple least squares approach that the recent CW is much smaller than before, implying that the CW is essentially unexcited in recent years (Figures 2-1b and 2-1c), while Zotov et al. (2022)

also pointed out the recent zero CW through singular spectrum analysis (SSA). We are also informed that the CW signal in super-conducting gravimeter data at Syowa Station, Antarctica, has been weakened since several years ago (Personal communications with Yuichi Aoyama, Unpublished data).

Although the CW must have been continually excited by the Earth's surface fluids for over a century, how can we interpret the recent un-excitation? Now that high-precision space geodetic data are available and that global Earth system modelling allows us to compute higher-quality AAM, OAM, and HAM data sets as the estimates of excitation, we examine if the present Earth system modelling data can explain the anomaly and discuss why the CW is not as extensively excited as before. Understanding the excitation and un-excitation processes of the CW will also have implications for polar motion prediction; the presence of freely damped CW, if any, will make the polar motion prediction much simpler because the CW dominates over the "rapid polar motion" with timescales between two weeks to several months (Eubanks et al. 1989). Earth rotation data including polar motion plays a significant role in the prediction of the orbits of artificial satellites and space probes. Even displacements of only a few centimetres in the motion of the rotation axis relative to the pole can lead to substantial differences when propagated to large distances from the Earth. Consequently, understanding Earth rotation variability such as polar motion and changes in the angular velocity of rotation is essential for sustaining and providing the fundamental geodetic data that underpin space utilisation.

II.II. Data and Methods

Polar motion data

We use the earth orientation parameter (EOP) data, EOP 14 C04 for the recent decades and EOP C01 going back to 1846 (Bizouard et al. 2019). Although the EOP 14 C04 provided daily data, it is available only for the period after 1962, when high-precision observations became feasible. To investigate the entire interval since 1846, including the era of optical observations, it is necessary to use the EOP C01 series, which is provided at intervals of 0.05 years. Because the AW does not change its phase by definition of the forced oscillation associated with seasonal excitation, and because its amplitude is nearly constant (Gross 2015), we can fit the polar motion data from 2015 to 2021 with a simple two-component model consisting of only the AW and secular drift (Figure 2-1); fitting the seasonal signals with constant-amplitude sinusoids is a conventional approach to studying the CW excitation (e.g., Gross 2000), and we approximate the secular drift with a second-order polynomial. Subtracting the two-component time series from the original data with an extension to 1971, we observe that the CW started to be weaker in 2005 and became insignificant in 2015 (Figure 2-1b). The post-2015 smaller-amplitude signals in Figure 2-1b will indicate either the so-called rapid polar motion (Eubanks et al. 1988) and/or the modulated amplitude in the AW and have to be distinguished from the previously observed CW; if the CW were present as previously even after 2015, we should have observed a 6-year beat in recent years as well. Extending the two-component model to 1890, we could reproduce and confirm the smaller CW in 1920-40 (Figure 2-1c). The post-2015 small amplitude in Figure 2-1b might well include some CW signals but no such small amplitude CW had been observed before. Thus, for simplicity, we refer to the post-2015 CW as the “absence”; even though the post-2015 CW amplitude is not exactly zero, our conclusions below do not change.

Polar motion theory and excitation functions

As described in Chapter I.III., theoretically, the Earth's wobble, $\tilde{p}(t) \equiv x(t) - iy(t)$, is considered to be generated through a convolution of an impulse response function, $e^{i\tilde{\sigma}_{cw}t}$ with excitation sources, $\tilde{\chi}(t)$:

$$\tilde{p}(t) = \tilde{p}_0 e^{i\tilde{\sigma}_{cw}(t-t_0)} - i\tilde{\sigma}_{cw} \int_{t_0}^{t} e^{i\tilde{\sigma}_{cw}(t-\tau)} \tilde{\chi}(\tau) d\tau \,. \qquad (2-1)$$

The first term indicates a freely damping term due to the cumulative excitations by the time $t = t_0$. The second term represents the wobble excited after $t = t_0$ (Munk and MacDonald 1960); the complex form for the pole position and excitation allows us to analyse the 2-D motion with 1-D data. Here, $x(t)$ and $y(t)$ indicate the location of the North Pole along the Greenwich meridian and the 90°West Longitude, respectively, and $\tilde{\sigma}_{cw} \equiv 2\pi/P\,(1 + i/2Q)$ is the complex characteristic frequency defined by P and Q. Conventional approach to examine the polar motion excitation is first to perform deconvolution of the observed data, $\tilde{p}(t)$ into "geodetic" excitation, $\tilde{\chi}_{geod}(t)$ with an assumed pair of P and Q (Wilson 1985). We can compute "geophysical" excitation, $\tilde{\chi}_{geoph}(t)$ independently from the $\tilde{\chi}_{geod}(t)$, using global Earth system modelling data that became available as AAM in the early 1980s (Barnes et al. 1983) and OAM in the late 1990s (Ponte et al. 1998); currently available AAM is all based on assimilation data, but some OAMs are not based on assimilation data even now. The AAM and OAM include both the mass (moment of inertia tensor) and motion (relative angular momentum) terms, where surface air and ocean bottom pressure changes contribute to the mass term, and atmospheric wind and ocean current contribute to the motion term. We assumed that the ocean surface responds to reduce variance of the air pressure, which is called an "inverted barometer". Nowadays, land water hydrological effect is also estimated as HAM based on the Land Surface Discharge Model (Dill 2008). After considering the effect of elastic response and core-mantle decoupling (e.g., Gross 2015), we can compare the "geodetic" excitation, $\tilde{\chi}_{geod}(t)$ with "geophysical" excitations, $\tilde{\chi}_{geoph}(t)$. Table 2-1 lists the geophysical excitation data sets in this study and Figure 2-2 is the flowchart to calculate $\tilde{p}_{geoph}$ and $\tilde{p}_{geod}$.

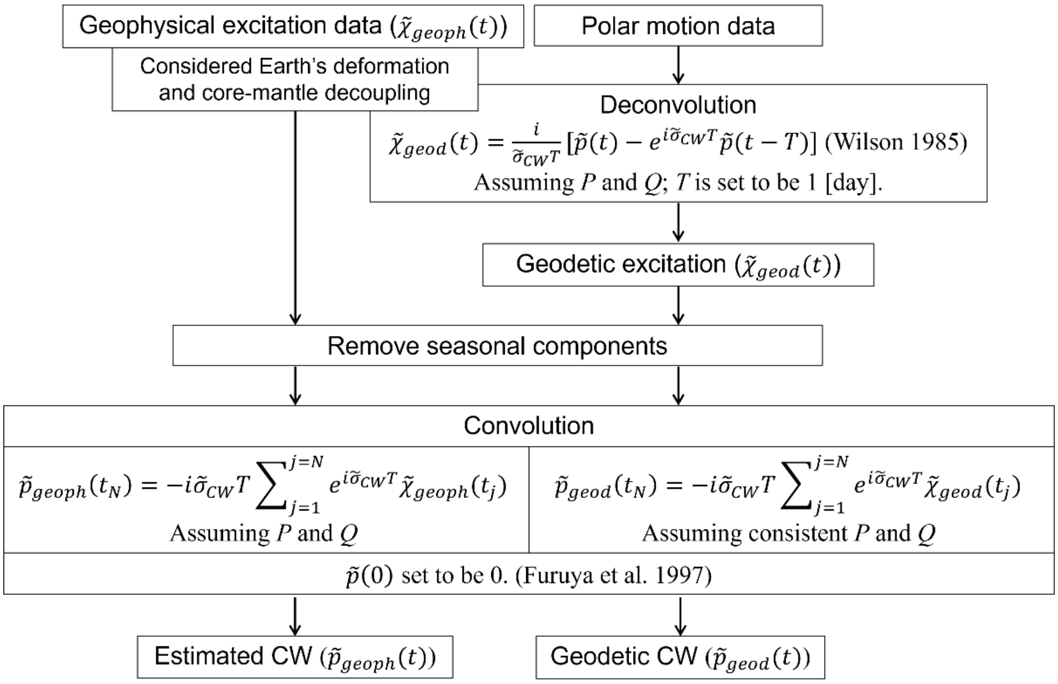

[Figure 2-2] A flowchart of the procedure to calculate $\tilde{p}_{\mathrm{geoph}}(t)$ and $\tilde{p}_{\mathrm{geod}}(t)$. We integrated the geophysical excitation ($\tilde{\chi}_{\mathrm{geoph}}$) after removing seasonal components to estimate CW ($\tilde{p}_{\mathrm{geoph}}$). Then, we set the initial value to be zero. In order to calculate $\tilde{p}_{\mathrm{geod}}$, we followed the same procedure for $\tilde{\chi}_{\mathrm{geoph}}$, which was calculated by deconvoluting the observed polar motion data.

[Table 2-1] Geophysical excitation data used in this study

Data	**Components**	**Data provided from**	**Period**

ESMGFZ (Dobslaw and Dill 2018)	Atmosphere + Ocean + Hydrosphere	Deutsches GeoForschungsZentrum (GFZ) from the original European Centre for Medium-range Weather Forecast (ECMWF) atmosphere, Max-Plank Institute Ocean Model (MPIOM), and the Land Surface Discharge Model (LSDM) data	1976-2021
JRA-55 (This study)	Atmosphere	Original JRA-55 data by Japan Meteorological Agency (JMA) (Kobayashi et al. 2015)	1960-2021
NCEP+ECCO (Salstein et al. 1993; Gross et al. 2003)	Atmosphere + Ocean	Paris Observatory from the original National Centre for Environmental Prediction (NCEP) atmosphere and the Estimating the Circulation and Climate of the Ocean (ECCO) ocean model data	1962-2021 (A) 1962-2018 (O)

Analysis approach in this study

Analysis approach in this study is to compare in the wobble domain. Performing the convolution with any geophysical excitations on the assumption of P and Q, we may compare the geodetic wobble, $\tilde{p}_{geod}(t)$ with the geophysical wobble, $\tilde{p}_{geoph}(t)$. For the analysis of the CW excitation sources, we think that the wobble domain approach performs better than the excitation domain approach because we can amplify any small excitation signals around the resonant frequency that essentially contribute to exciting the CW (Furuya et al. 1997). Although the same conclusion should be drawn in theory, we are led to compare small amplitude signals in both geodetic and geophysical data in the excitation domain. Moreover, performing the comparison in frequency domain as many previous studies (e.g., Furuya et al. 1996; Gross 2000; Aoyama and Naito 2001), the frequency resolution is seriously limited by the available data length. Nonetheless, most previous studies have circumvented the wobble domain approach because the first term in Eq. (2-1) represents a free damping that generates a non-zero CW amplitude even without any excitations afterward (Chao 1985). However, if we start the convolution with zero initial value, we can more directly evaluate if and how much the candidate sources can excite and maintain the CW. Chao (1985) did not mention another caveat for the wobble domain analysis. Namely, we must take out the seasonal signals before convolution (integration) because, even if the integration starts from zero initial value, a sudden start of large seasonal forcing will generate a transient CW that is not present in actual data. Such a transient CW is cancelled by a damped CW excited by seasonal forcing; seasonal forcing eventually generates only seasonal wobble in a linear dynamical system. The resulting solution of the Liouville equation, with the annual forcing substituted as the external forcing, can be expressed as:

-

$$p = p(0)\exp[i\tilde{\sigma}_{CW}t] + \frac{\tilde{\sigma}_{CW}}{\tilde{\sigma}_{CW}-\omega_a}\chi_a \exp[i\omega_a t], \qquad (2-2)$$

where $\omega_a = 2\pi/365.25$ and χ_a is the amplitude of the annual forcing. This implies that the annual forcing only excites the AW because the initial condition is set to $p(0) = 0$. The geodetic CW can thus be derived by re-convolving (re-integrating) the deconvolved non-seasonal geodetic excitation with the same P and Q (Furuya et al. 1997). The drawback in the wobble domain approach is that there arises the same issue as the "non-zero" initial value when the integration time is extended. However, it also depends on the time scale of the damping of CW, i.e., prescribed *Q*; precision estimation of CW's *Q* is therefore important.

II.III. Results

Sensitivity of the results to *P* and *Q*

To demonstrate the sensitivity of $\tilde{p}_{geod}(t)$ and $\tilde{p}_{geoph}(t)$ to the assumed *P* and *Q*, Figure 2-2 shows five cases of the *x* component from $\tilde{p}_{geod}(t)$ and $\tilde{p}_{geoph}(t)$ with different pairs of *P* and *Q*. To compute $\tilde{p}_{geoph}(t)$ by $\tilde{\chi}_{geoph}(t)$ in Figure 2-2, we summed up the AAM, OAM, and HAM provided by the Earth System Modeling Group at GFZ (ESMGFZ) in Table 2-1 that computed the total angular momentum changes within the Earth's surface fluid system most comprehensively. Notably, $\tilde{p}_{geod}(t)$ indeed show a much smaller amplitude after 2015, whereas the amplitude and phase also depend on the pair of *P* and *Q*. Moreover, we observe that $\tilde{p}_{geoph}(t)$ varies sensitively to the assumed pair of *P* and *Q*, and thus we can tightly constrain optimum *P* and *Q* by matching $\tilde{p}_{geod}(t)$ and $\tilde{p}_{geoph}(t)$ (Figure 2-3). The discrepancies between $\tilde{p}_{geod}(t)$ and $\tilde{p}_{geoph}(t)$ suggest either that the pair of *P* and *Q* is inadequately assumed or that any of $\tilde{\chi}_{geoph}(t)$ still incompletely captures the real geophysical excitations or both. However, based on the currently available data, we may claim that optimum *P* is 432 days and that *Q* is unlikely to be as high as 100, judging from Figure 2-3e. Although the smallest *Q* of 25 better matches the post-2015 smaller signal (Figure 2-3b), there are significant discrepancies from the 1980s to the early 2000s (Figure 2-3d).

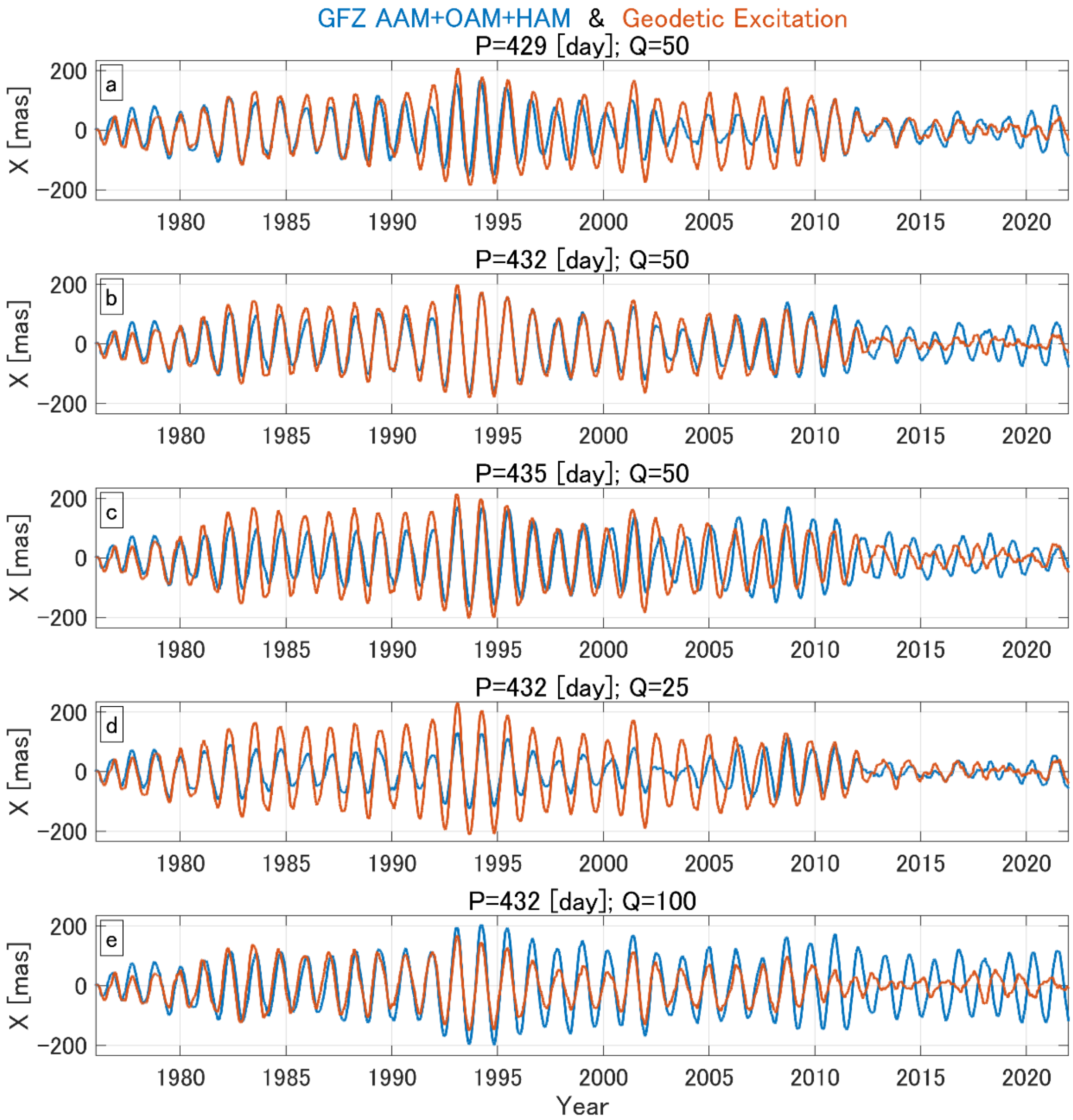

[Figure 2-3] Comparisons of the estimated geodetic and geophysical CW as a function of P and Q (X-component). (a) P = 429 days, Q = 50, (b) P = 432 days, Q = 50, (c) P = 435 days, Q = 50, (d) P = 432 days, Q = 25, (e) P = 432 days, Q = 100.

Can the available geophysical data reproduce the recent CW?

To account for the recent absence of the CW, we may conceive various scenarios in each of the AAM, OAM, and HAM contributions, respectively. For instance, all three contributions since 2015 may be equally smaller than before. Or alternatively, the total sum of the three contributions could happen to cancel each other and become nearly zero, whereas each of them might have substantial amplitude even after 2015. We examine in the wobble domain the contributions from three AAM (Figures 2-4a-2-4c), two OAMs (Figures 2-4d and 2-4e) originally driven by the same atmospheric data in Figures 2-4a and 2-4b, and one HAM (Figure 2-4f) estimated from the Earth system modelling along with Figures 2-4a and 2-4d (Dobslaw et al. 2010). We fixed *P* and *Q* with 432 days and 50, derived from the results in Figure 2-3. Although the AAM alone is not enough to explain the CW from the 1970s to 1990s (Figures 2-4a-2-4c), we observe that the three AAMs are roughly consistent with each other in terms of both amplitude and phase of the computed CW, and two of them further indicate persistently smaller amplitude since 2015 (Figures 2-4a and 2-4c).

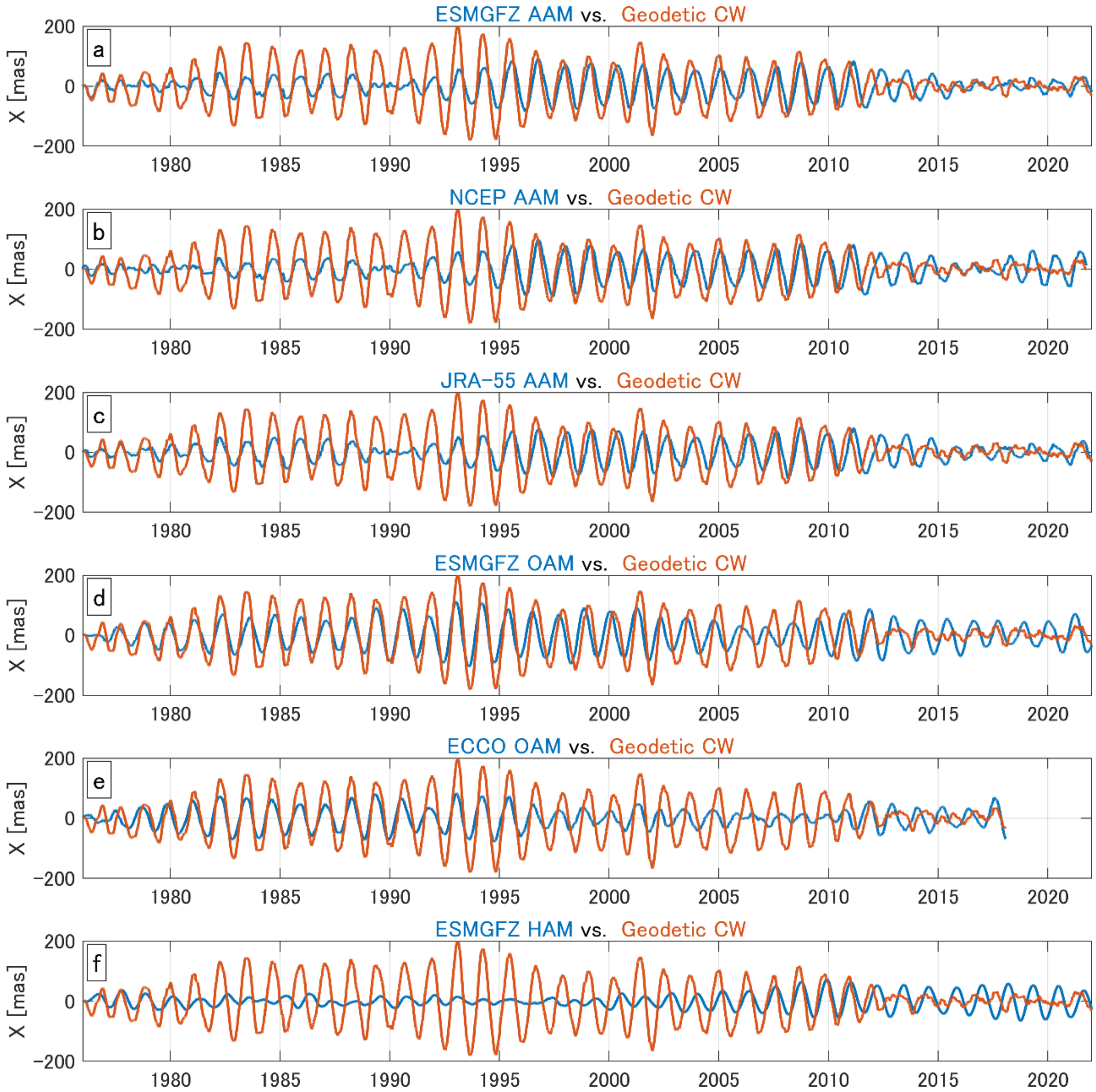

[Figure 2-4] Contributions to the estimated CW from each geophysical excitation data (X-component). Case with P = 432 days and Q = 50 for (a) ESMGFZ AAM, (b) NCEP AAM, (c) JRA-55 AAM, (d) ESMGFZ OAM, (e) NCEP/ECCO OAM, and (f) ESMGFZ HAM.

On the other hand, the two OAMs are not as consistent as the three AAMs and do not significantly change the amplitude even after 2015 (Figures 2-4d and 2-4e). Moreover, the HAM generates rather a greater CW in the recent period (Figures 2-4d-2-4f) and seems responsible for the significant discrepancies after 2015 in Figure 2-3b. We thus recognize that the available OAM and HAM may still include some errors and biases (Figure 2-4), whereas the two AAMs (Figures 2-4a and 2-4c) are almost in perfect agreement. It is uncertain if both the OAM and HAM have become smaller or if they have been cancelling each other since 2015.

Contributions from atmospheric mass and motion terms

To investigate the reason why the atmospheric contribution decreased in 2015, we analyse the JRA-55 AAM for the matter and motion terms separately. Figure 2-5 shows the integrated AAM of the matter term and the motion term, respectively. The phases of the matter term and the motion term became inverted after 2015, when the CW was absent; as the matter term and motion term cancelled each other out, the overall atmospheric contribution became smaller.

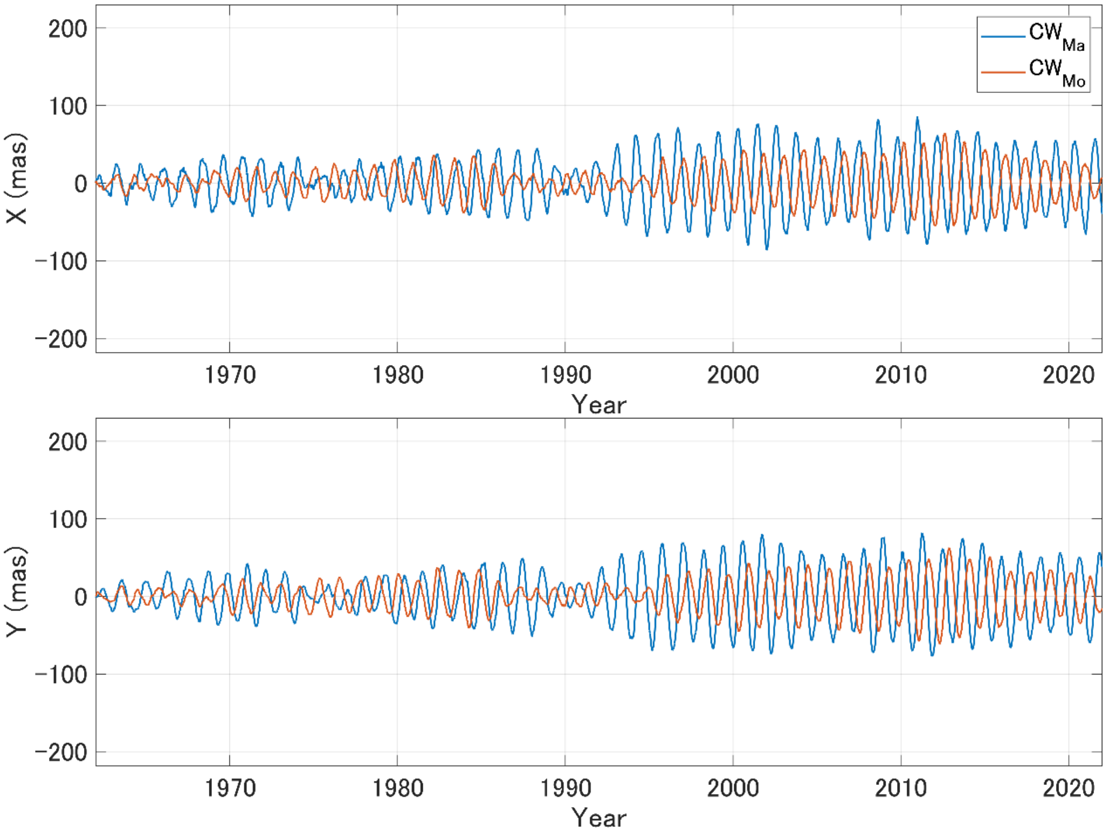

[Figure 2-5] Integrated JRA55 AAM of the matter term (blue) and the motion term (red) assuming P = 432 days and Q = 50.

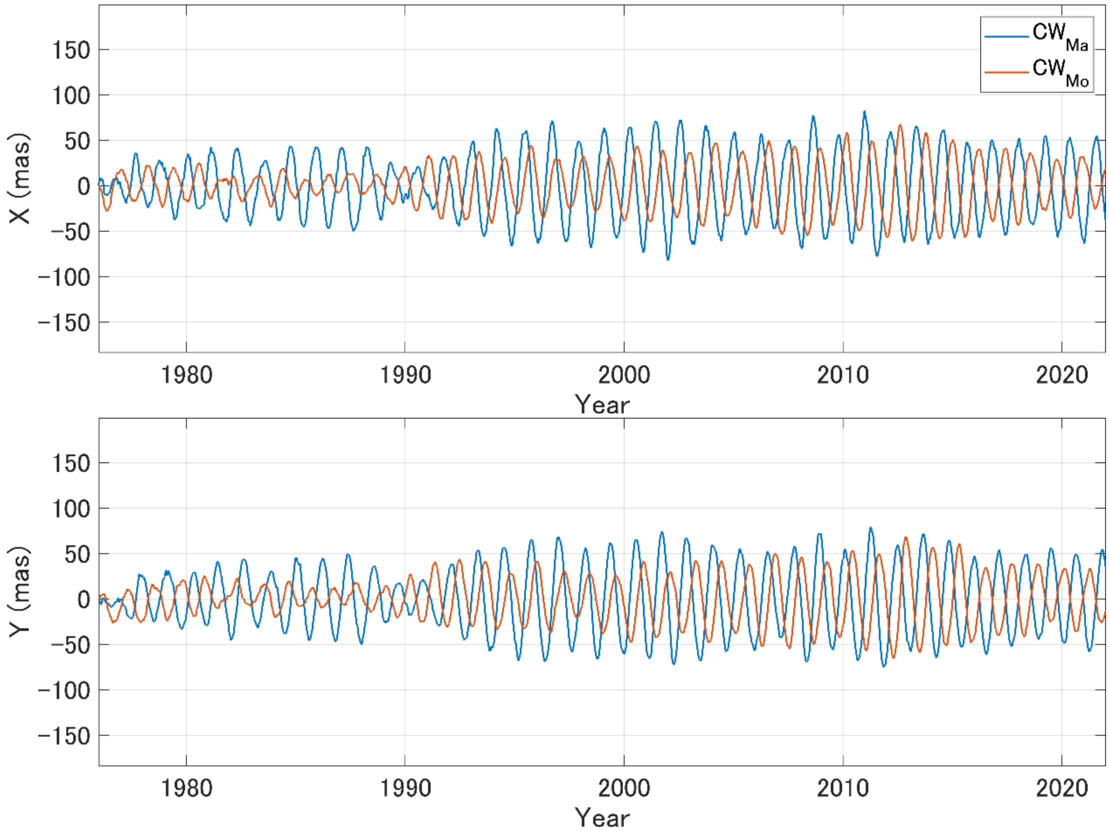

[Figure 2-6] Integrated ECMWF AAM of the matter term (blue) and the motion term (red) assuming P = 432 days and Q = 50.

Latitudinal contributions of JRA-55 AAM

In addition, the JRA-55 AAM is divided into 15-degree latitudinal zones to examine the regional contribution of the atmosphere, Figures 2-5 and 2-6 show integrated AAM of the matter term and motion term separated by latitude, respectively.

Overall, the matter term has a smaller contribution than the motion term. In the southern mid-latitude zone, i.e., 45°S-75°S, the contribution is significantly larger than in the other zones (Figure 2-7) even when taking into account that lower latitudes are greater weighted than higher latitudes.

Comparing each zone, the phase differences among the zones are generally small. Because of the small phase differences, the contribution as a whole becomes larger, about 50 mas, when they are integrated.

On the other hand, the contribution of the motion term varies across the latitudinal zones. Figure 2-8 shows the integrated latitudinal JRA-55 AAM of the motion term. The amplitude of the integrated value of the motion term is larger than that of the matter term in all zones. In addition, both the amplitude and the phase differ among the zones. In some cases, the motion term has an even larger amplitude after 2015 than before. The result suggests that the reduction of the atmospheric contribution after 2015 is mainly derived from the behaviour of the wind in the mid-latitude zones.

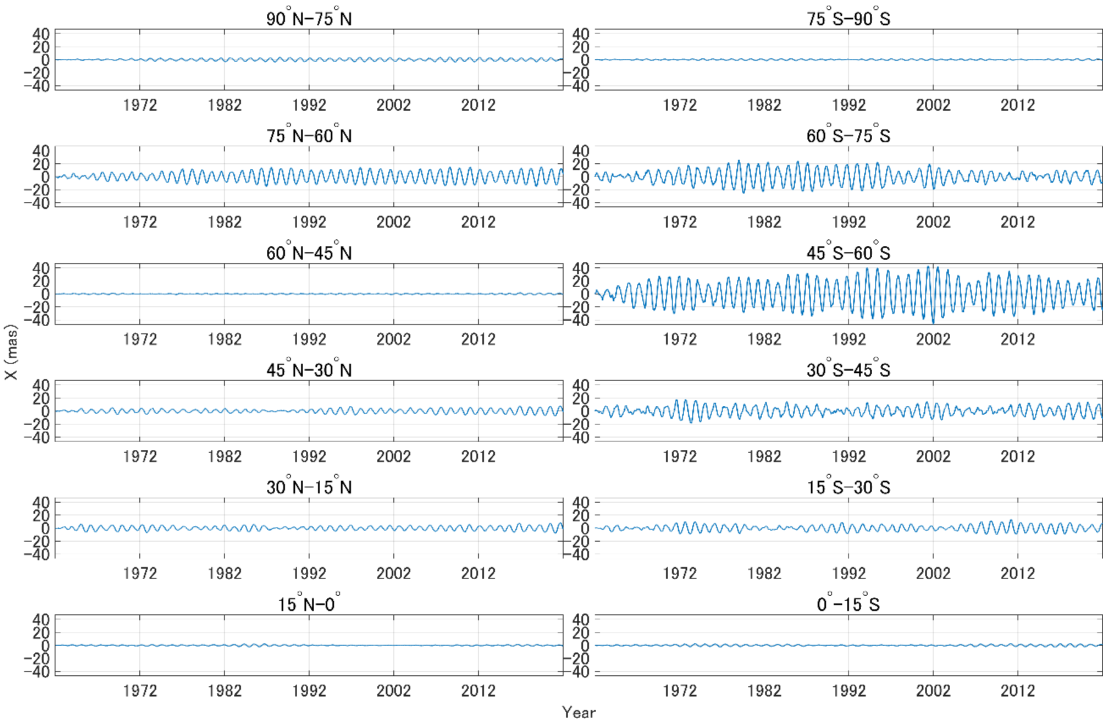

[Figure 2-7] Integrated latitudinal AAM of the matter term, the integrated value (blue) and the observed value (red).

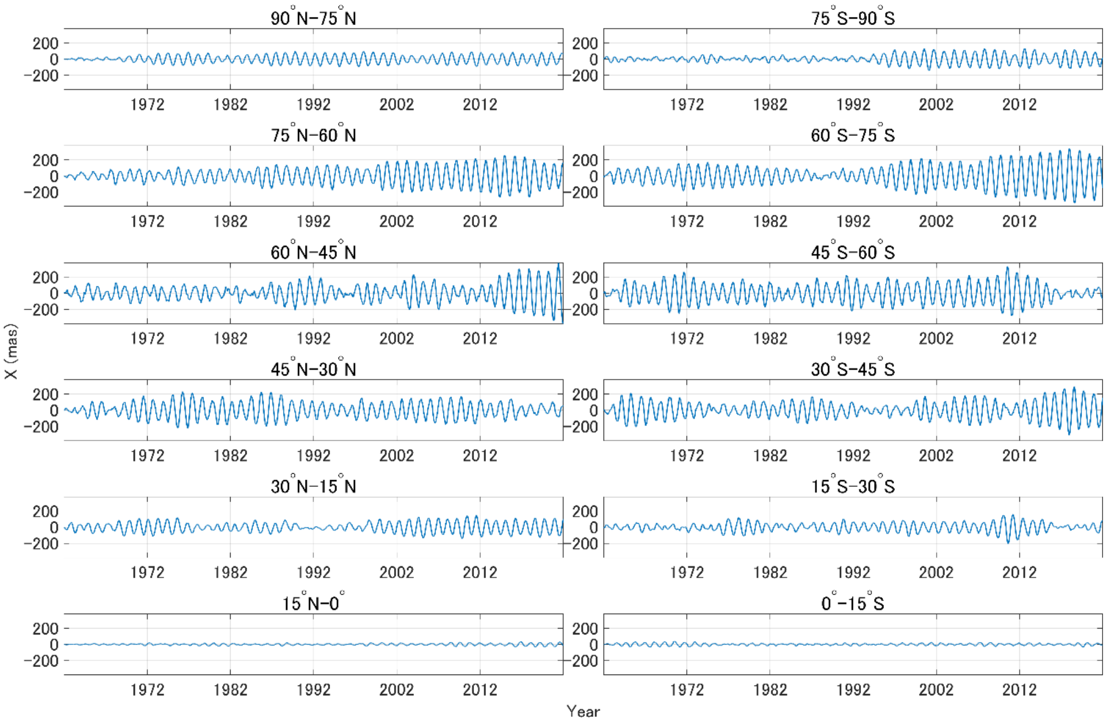

[Figure 2-8] Integrated latitudinal AAM of the motion term, the integrated value (blue) and the observed value (red)

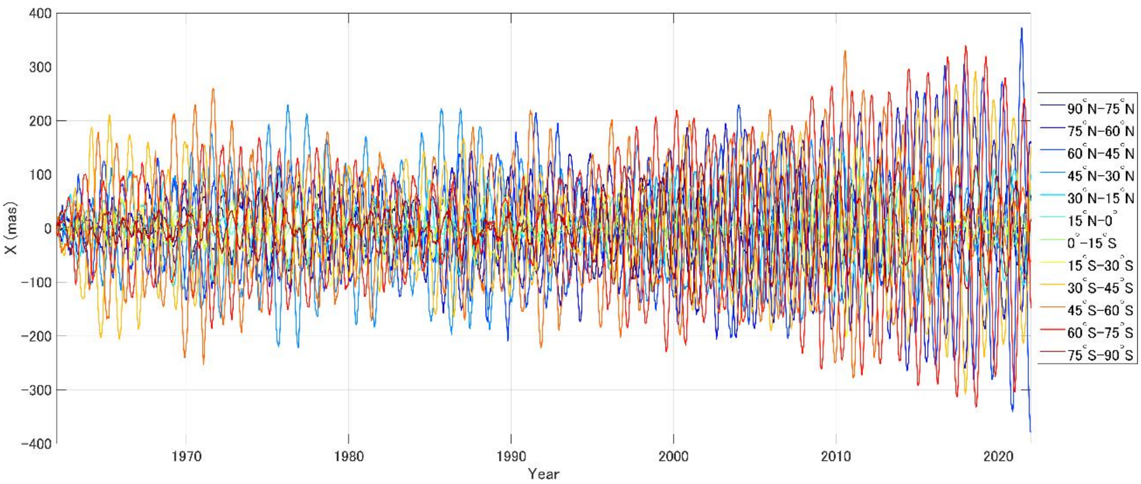

[Figure 2-9] Integrated latitudinal AAM of the motion term, shown for each 15-degree latitudinal zone from north (blue) to south (red).

II.IV. Discussions

Implications of the recent CW anomaly for excitation processes and global warming

Figures 2-1a and 2-1b indicate that the CW started to become smaller in ~2005 and almost disappeared in 2015. We may recall the shift in the direction of the secular polar drift to the east since ~2005, which was attributed to the rapid ice melting in Greenland (Chen et al. 2013). However, the effect of abrupt ice melting will have more impact in the lower frequency than around the Chandler frequency and thus is not directly related to the CW absence. Nonetheless, we consider that both anomalies in the secular drift and the CW would be more or less associated with the recent global warming trend. It is not straightforward, however, to relate the trend to the CW absence.

Why is the CW not excited since 2015? Regarding the excitation processes of the CW, it is still an open question whether they are random or nearly resonant. Numerous previous studies on the CW excitations have assumed (or believed) the Gaussian random process (e.g., Okubo 1982; Chao 1985; Chao and Chung 2012), and the random excitation model will regard the post-2015 CW anomaly as "simply fortuitous by chance" (Chao and Chung 2012). However, if we took a simple analogy with the classical thermal-noise model, global warming would increase the noise level and amplify the CW, which conflicts with the observation. On the other hand, several earlier studies instead suggested a near-resonant excitation, in which the CW has been maintained by quasi-periodic excitation with a characteristic period of ~14 months in the atmosphere (Furuya et al. 1996; Plag 1997; Aoyama and Naito 2001; Aoyama et al. 2003) and the ocean (Plag 1997); note that those studies do not claim that the polar motion follows a non-linear dynamical system. The CW absence may be interpreted as an abrupt termination of such processes. The recent persistently smaller AAM contributions in Figures 2-4a and 2-4c are for the first time in decades and seem to be in accord with this model; the three

AAM time-series data are nearly identical to each other (Figure 2-10), and the deviation of Figure 2-4b would be due to the small but different spectral content around the Chandler frequency. Although the periodicity of ~14 months is unclear in Figures 2-4a-2-4c, even a small amplitude is enough if it is close to P, and its amplitude needs not to be constant, either. Moreover, any near-resonant excitation sources, if any and not limited to AAM, can more easily excite the CW even with the lower Q.

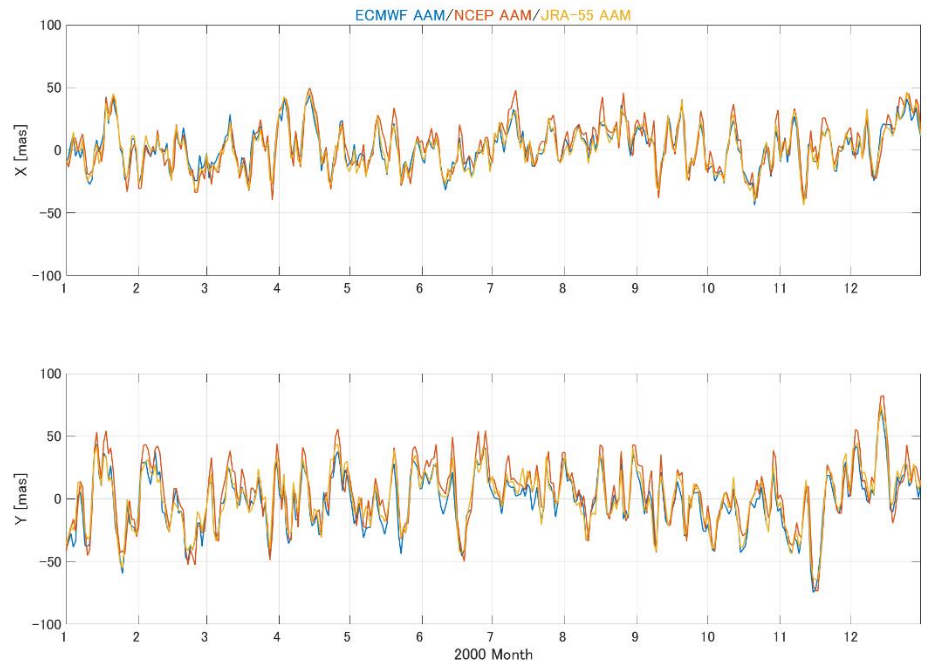

[Figure 2-10] Comparisons of ECMWF (blue), NCEP (red), and JRA-55 AAM (yellow) in 2000. The annual component and the quadratic long-term motion are removed from all data. The NCEP AAM data were shifted by three days from the original data available from Paris observatory.

Concerning the recent smaller atmospheric excitation, we note the disruption of the equatorial quasi-biennial oscillation (QBO) in the 2015/2016 winter (Osprey et al. 2016; Newman et al. 2016) and 2019/2020 winter (Antsey et al. 2021), which have never been observed before, either. As the QBO itself is zonal wind oscillation in the tropics with a mean period of 28 months (Baldwin et al. 2001), it only affects the length-of-day change (Chao 1989), and no corresponding periodicity should be expected in the polar motion. However, the atmospheric circulation system associated with the QBO would not be strictly longitudinally symmetric and can affect the equatorial angular momentum budget that also includes meridional winds; the role of meridional momentum transport is indeed pointed out for the recent QBO disruptions (Osprey et al. 2016; Newman et al. 2016; Antsey et al. 2021). Although the dynamical relations between the QBO and the ~14 months oscillations in AAM are unclear now, the recent smaller AAM in Figures 2-4a and 2-4c is possibly associated with the QBO disruptions. Similar QBO disruptions are predicted in several climate models under warming scenarios (Osprey et al. 2016; Antsey et al. 2021). The meteorological origins of the recent smaller AAM contributions in Figure 2-4 are uncertain and need further examination in detail.

II.V. Summary

Although polar motion data have exhibited a 6-year beat for over a century, it has been absent since 2015. We examined if the available estimates of atmospheric, oceanic, and land-water excitation could reproduce the anomaly. It turned out that atmospheric CW excitation became persistently smaller than before but that the estimates of those oceanic and land-water contributions were not consistent enough, suggesting further room to improve their accuracies. Taking advantage of the recent CW anomaly, we show that the quality factor of CW is not as high as the previously preferred 100, indicating that the required CW excitation power is higher than expected before. Although the CW excitation processes have been widely assumed to be random, the recent absence might indicate a termination of more coherent excitation processes.

III. OCEANIC CONTRIBUTION TO THE ABSENCE OF THE CW

III.I. Introduction

Yamaguchi and Furuya (2024) demonstrates that the CW was absent from 2015 and that the atmospheric contribution to its excitation was reduced over the same period. On the other hand, Xu et al. (2024) states that the absence of the CW occurs because the atmospheric and oceanic contributions cancel each other out, based on the integration of the NCEP AAM and the ECCO OAM. However, as shown in Figure 2-4, the integrated ECCO OAM is not consistent with the integrated MPIOM OAM. Moreover, of the three AAMs, i.e., NCEP, ERA-5, JRA-55, both ERA-5 and JRA-55 are nearly identical, but NCEP AAM shows some differences from the other two AAMs. It suggests that a new OAM, derived from an independent ocean model driven by another atmospheric data, is required to clarify the oceanic contribution.

In this study, we newly compute an OAM based on the OFES2 model data provided by JAMSTEC (Sasaki et al. 2020). We aim to assess the contribution of the ocean to the excitation of the CW clearly using the OFES2 OAM. We also expect that the OFES2 can complement the JRA-55 AAM because the JRA

III.II. Data and Methods

The OAM is calculated based on the OFES2 model provided by the JAMSTEC (Sasaki et al. 2020). The OFES2 model is driven by the JRA-55 atmospheric reanalysis data as one of the sources, which enables a complementary assessment of the atmospheric contribution previously estimated from the JRA-55 AAM first computed in Yamaguchi and Furuya (2024). The dataset spans the period from

1958 to 2023, and the monthly data was used here as a preliminary experiment. The monthly data are helpful enough to examine the contribution to the excitation of CW, because the CW is most effectively excited by the power around the resonant frequency.

The OAM is calculated separately for the matter term and motion term in the same procedure as the AAM. The matter term reflects changes in the product of inertia due to mass redistribution of seawater.

Therefore, the excitation of the matter term is calculated by integrating the ocean bottom pressure p_b as:

$$\chi_{Ma} = -\frac{1.100\, a^4}{(C - A')} \int_{-\frac{\pi}{2}}^{\frac{\pi}{2}} \int_0^{2\pi} p_b \sin\phi \cos^2\phi \exp(i\lambda)\, d\lambda d\phi\,, \qquad (3-1)$$

where a is the mean radius of the Earth, A' and C are equatorial and axial principal moments of inertia of the Earth, respectively, g is the gravitational acceleration, ϕ is latitude, and λ is longitude (Börger et al. 2025).

On the other hand, the motion term reflects changes in relative angular momentum due to the ocean currents. Thus, for the calculation of the motion term, the water currents speeds (u for westerly and v for southerly) on all isobars are integrated as:

$$\chi_{Mo} = -\frac{1.608\, a^3 \rho_0}{\Omega(C - A')} \int_{-\frac{\pi}{2}}^{\frac{\pi}{2}} \int_0^{2\pi} \int_{-H}^{0} (v \sin\phi + iu) \cos\phi \exp(i\lambda)\, dz d\lambda d\phi\,. \qquad (3-2)$$

The procedure we used to estimate p_b follows Quinn et al. (2019) as:

$$p_b(\phi, \lambda) = \left[\rho_0 \eta + \int_{-H}^{0} \rho(\phi, \lambda, z) dz + SI + GC\right] g, \qquad (3-3)$$

where ρ_0 is the mean density, η is the sea surface height, and ρ is the in-situ density of the seawater. The term "SI" stands for the sea ice and snow loads, and "GC" stands for the Greatbatch correction described later. We adopted the equation of state, TEOS-10 (IOC et al. 2010), to estimate the in-situ density, and we used the Gibbs SeaWater Oceanographic Toolbox of TEOS-10 (McDougall and Barker 2011).

Firstly, the pressure of each isobar is estimated from the depth. Next, the absolute salinity is calculated from the pressure and the practical salinity data. To calculate the in-situ density, the conservative temperature, rather than the potential temperature, should be calculated using the absolute salinity and the potential temperature. Finally, the in-situ density is obtained using the absolute salinity, conservative temperature, and the pressure. The seawater loads and the Greatbatch correction are derived from the in-situ density. The flow chart of the overall procedures is shown in Figure 3-1.

The sea-ice and snow loads are estimated as:

$$SI = (\rho_{ice}\eta_{ice} + \rho_{snow}\eta_{snow})\mathcal{I}, \qquad (3-4)$$

where ρ_{ice} and ρ_{snow} are density of ice and snow, respectively, η_{ice} and η_{snow} are ice and snow surface thickness, respectively, and $\mathcal{I}$ is the ice concentration ratio from 0 to 1.

In addition, to account for the interaction between the atmosphere and the ocean, the Greatbatch correction (GC; Greatbatch, 1994) is required to eliminate the effects of the Boussinesq approximation adopted in the ocean model. Under the Boussinesq approximation, the density changes of the seawater are represented only through thermal expansion and contraction, rather than through true volume changes. To take the inverted barometer effect into consideration, not volume but mass should be conserved. The Greatbatch correction is calculated as:

$$GC = \frac{1}{A}\int_A \int_{-H}^{0} (\rho - \rho_0)\,dz\,dA, \qquad (3-5)$$

where A is the area of the ocean.

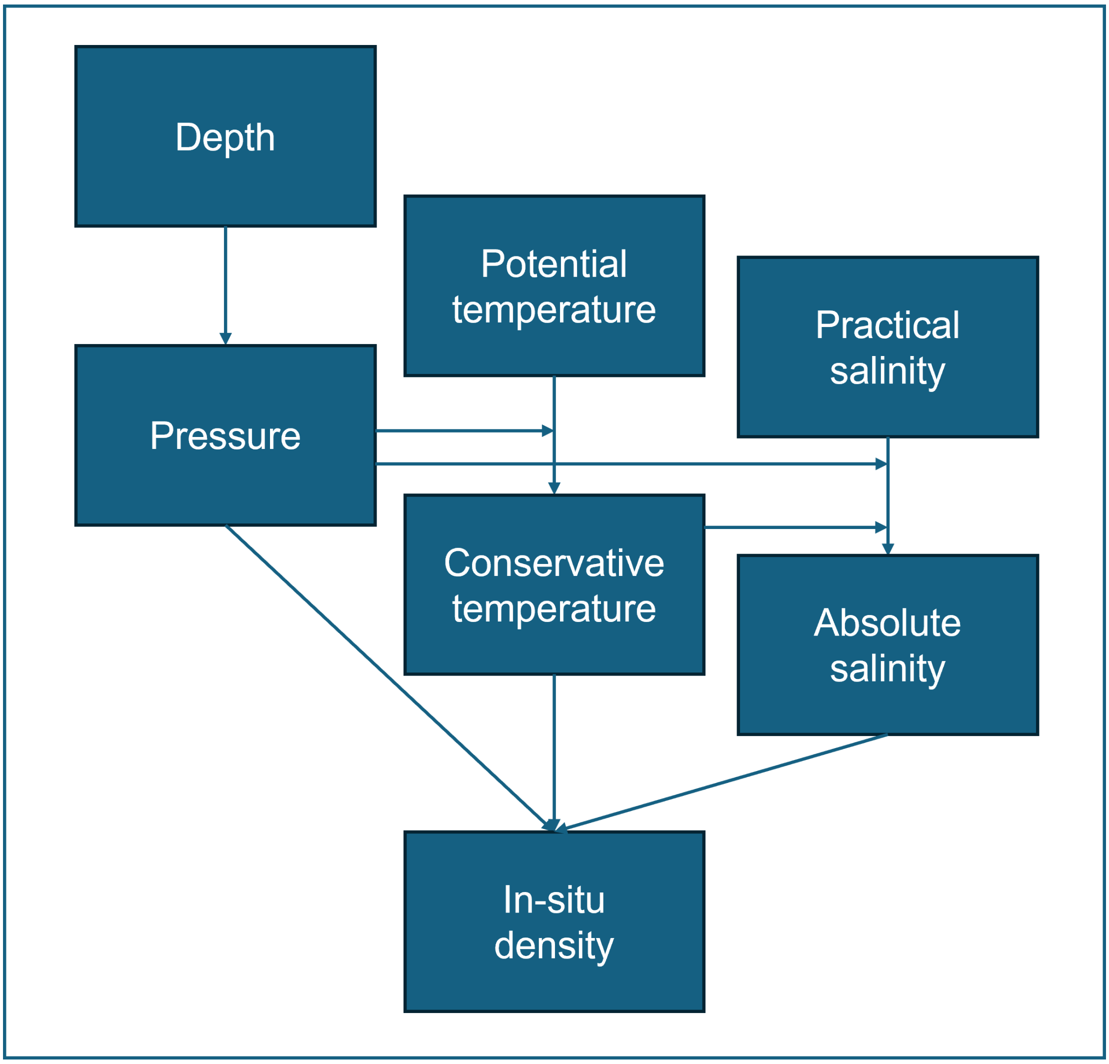

[Figure 3-1] Flow chart of the procedure used to calculate the in-situ density. The ocean bottom pressure is obtained by integrating the in-situ density of the seawater.

III.III. Results

Figures 3-2 and 3-3 show the comparison of the motion and matter term of the three OAMs, respectively. In terms of the motion term, the OFES2 OAM is in good agreement with the other OAMs. The mean amplitude of the motion term of each OAM from 1976 to 2017, when all data are available, is 7.04 mas (OFES2 OAM), 9.38 mas (MPIOM OAM), and 6.39 mas (ECCO OAM). The amplitude of the OFES2 OAM is closer to that of the ECCO OAM, at about 60% of the MPIOM OAM. On the other hand, the OFES2 OAM is about twice as large as the other OAMs regarding the matter term. The mean amplitude of the matter term of each OAM from 1976 to 2017 is 26.19 mas (OFES2 OAM), 13.30 mas (MPIOM OAM), and 9.90 mas (ECCO OAM). The three OAMs are found to be inconsistent with each other as a whole. One possible reason for this inconsistency is the differences in p_b. Therefore, we compared the p_b calculated from the OFES2 and ECCO ocean models in the Discussion section.

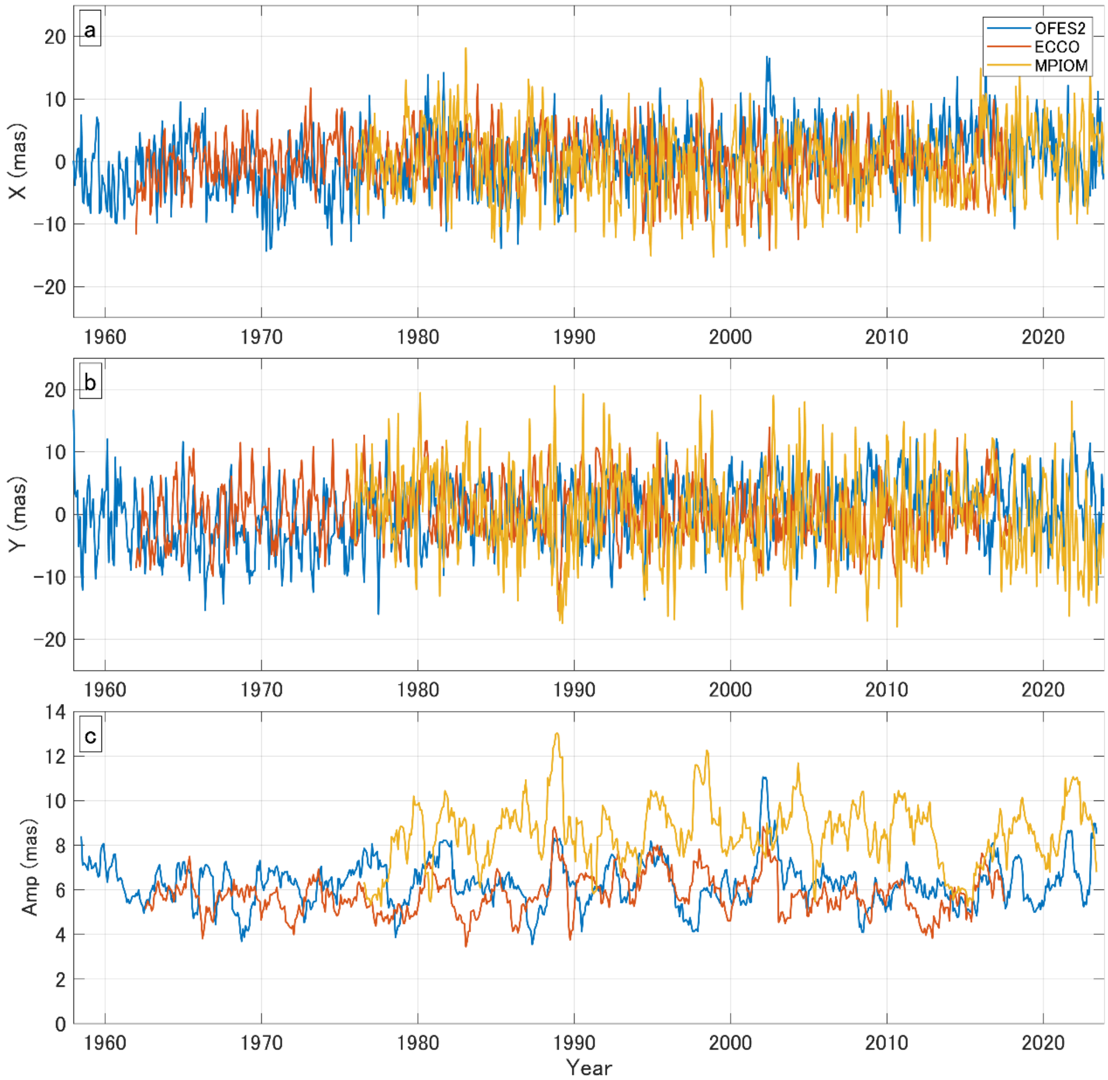

[Figure 3-2] (a), (b) The time-series of the motion term of the OFES2 OAM (blue), the ECCO OAM (red), and the MPIOM OAM (Yellow) X components for (a), Y components for (b). (c) the annually averaged amplitude.

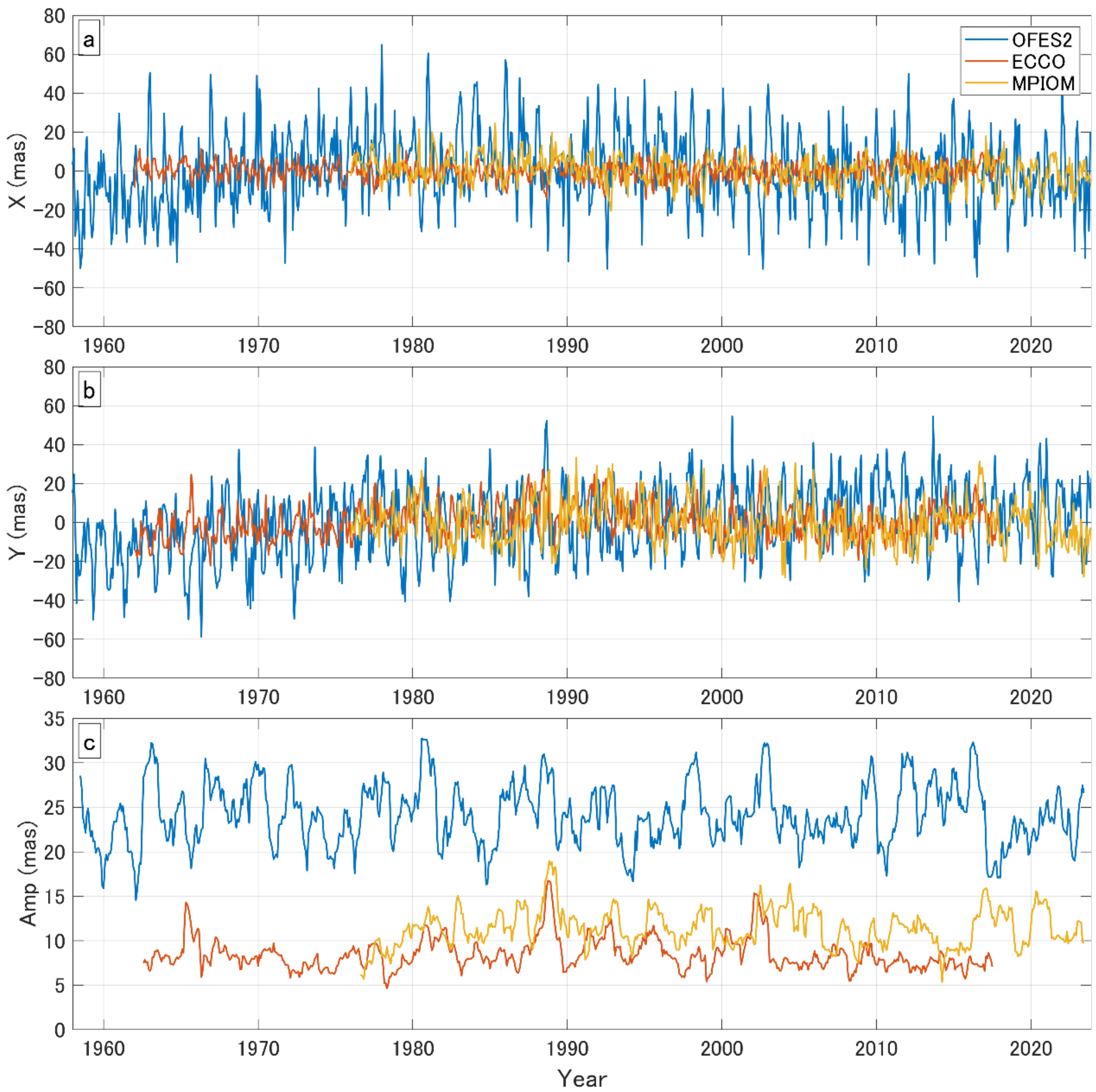

[Figure 3-3] (a), (b) The time-series of the matter term of the OFES2 OAM (blue), the ECCO OAM (red), and the MPIOM OAM (Yellow) X components for (a), Y components for (b). (c) the annually averaged amplitude.

III.IV. Discussion

Comparison of the p_b between OFES2 and ECCO

We compared the p_b between the OFES2 and ECCO models. Because the ocean bottom pressure data of the ECCO are provided as the equivalent water thickness (EWT):

$$\mathrm{EWT} = \frac{p_b}{\rho_0 g} - H + [\mathrm{Greatbatch\ correction}], \qquad (3-6)$$

we used the EWT instead of the p_b. The EWT data of ECCO from 1992 to 2018 are provided (ECCO Consortium et al. 2021). Figure 3-4 shows the map and the scatter plot of the two EWTs, indicating that the two p_b fields are in good agreement. However, the range of the correlation and its tendency vary depending on the region. Figure 3-5 shows the correlation, the coefficient, and the intercept when the approximating the ECCO p_b as a linear function of the OFES2 p_b. The results show that the regions with high correlation are limited, mainly the low-latitude or coastal zones. In the other regions, the correlation is weak or even negative. Considering over the entire ocean, OFES2 p_b tends to exhibit larger values than those of ECCO p_b. This suggests that the larger estimated p_b leads to the amplitude of the OFES2 OAM. A possible explanation for the p_b discrepancies is that the OFES2 ocean model is not synchronised with the observational data, whereas the ECCO model is assimilated with observational data as described in Chapter I.V. Although the OFES2 domain is limited to the region between 76°S and 76°N, the effect of the polar regions accounts for only 1.4% relative to the other regions, owing to the latitude weighting in Eq. (3-1). Nevertheless, additional and more detailed investigations will be required to ascertain the precise causes of this discrepancy fully.

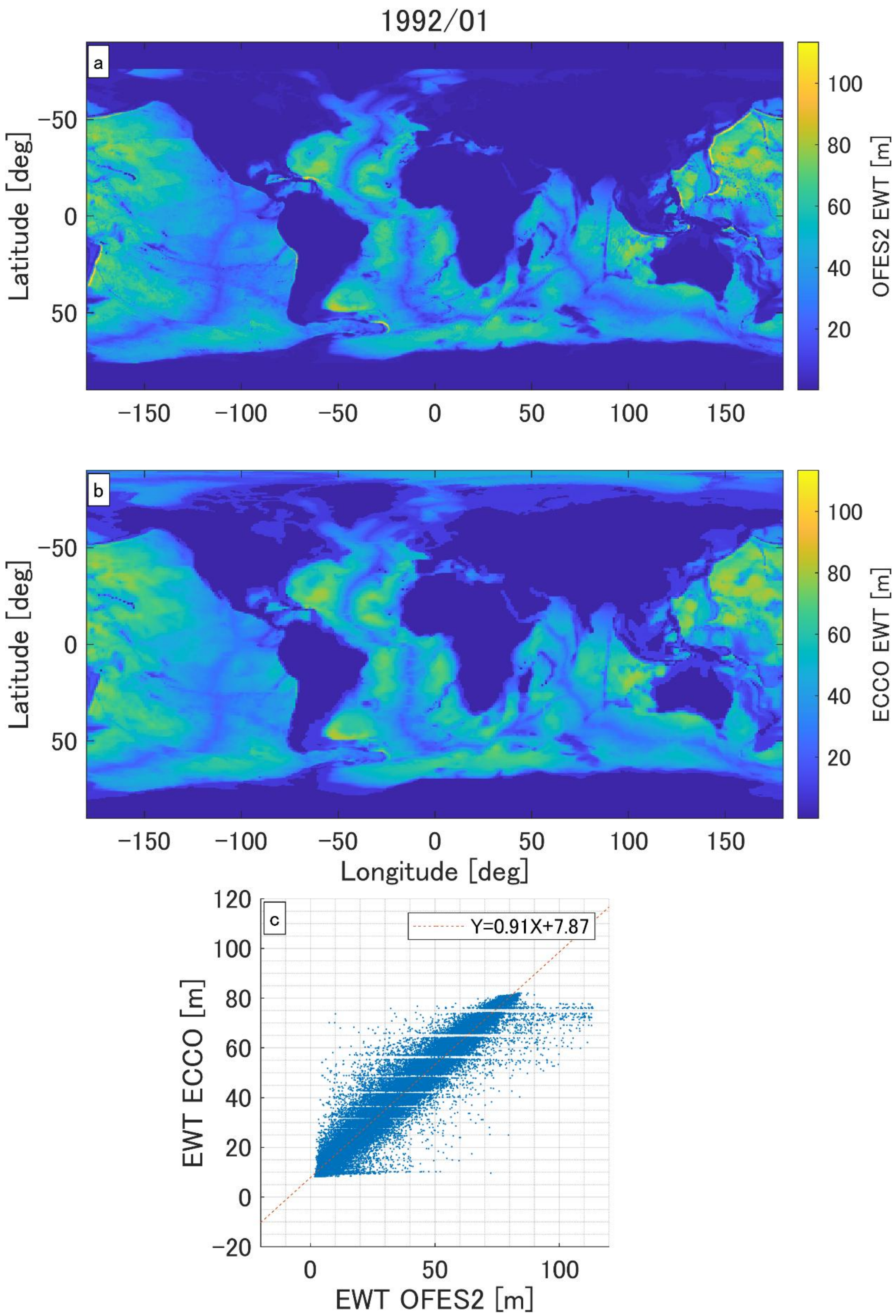

1992/01
a
Latitude [deg]
-50
0
50
-150
-100
-50
0
50
100
150
OFES2 EWT [m]
100
80
60
40
20
b
Latitude [deg]
Longitude [deg]
ECCO EWT [m]
c
Y=0.91X+7.87
EWT ECCO [m]
120
100
80
60
40
20
0
-20
EWT OFES2 [m]
0
50
100

[Figure 3-4] (a) The comparison between the OFES2 EWT and the ECCO EWT. (b) The scatter of the OFES2 EWT (horizontal) and the ECCO EWT (vertical) in January 1992.

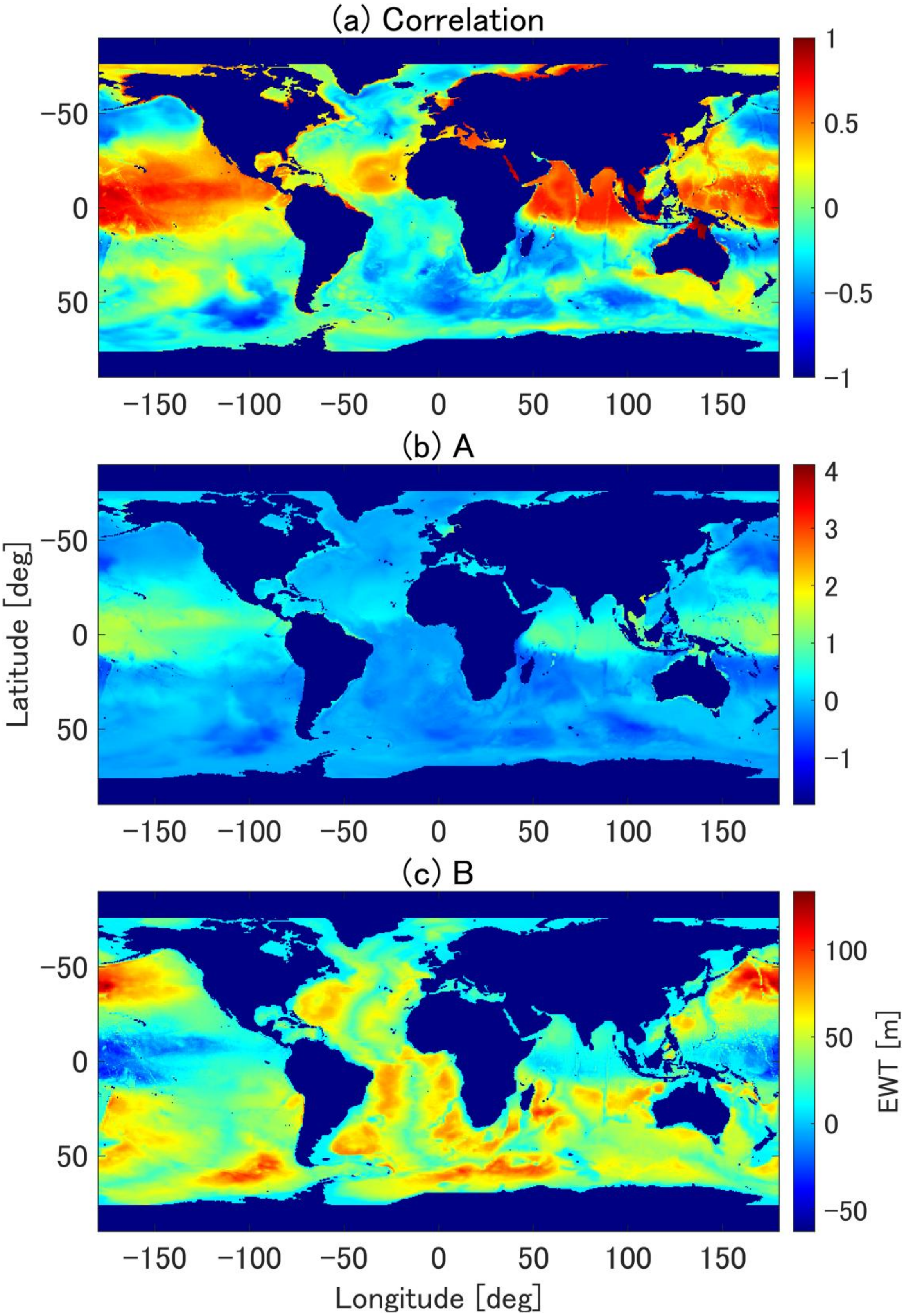

(a) Correlation
-50
0
50
-150
-100
-50
0
50
100
150
1
0.5
0
-0.5
-1
(b) A
Latitude [deg]
4
3
2
1
0
-1
(c) B
EWT [m]
100
50
0
-50
Longitude [deg]

[Figure 3-5] (a) Correlation of the OFES2 EWT and the ECCO EWT from January 1992 to December 2017. (b) Coefficient A and (c) intercept B when the ECCO EWT is approximated as a linear function of the OFES2 EWT, that is $[\text{ECCO EWT}] = A\,[\text{OFES2 EWT}] + B$.

III.V. Summary

To estimate the precise contribution of the ocean to the excitation of CW, a new OAM based on the OFES2 data was calculated. This represents the third OAM, which can be combined with the AAM. For the motion term of the OAM, there is not much difference among the three OAMs, and the amplitude of the OFES2 OAM is closer to that of the ECCO OAM. On the other hand, the matter term of the OFES2 OAM is almost twice as large as that of the other OAMs. Therefore, the three OAMs are found to be inconsistent with each other.

The p_b calculated from the OFES2 model data is in good agreement with that from the ECCO model data. However, the correlation between the two p_b fields depends on the region. Regions with high correlation are concentrated in the low-latitude zone, and in most of these regions the OFES2 p_b is larger than the ECCO one in most of the region. On the other hand, in the other regions the correlation is weak or even negative. Since there is significant weighting in the low-latitude zone when integrating to calculate the matter term, the OFES2 OAM could have larger amplitude than the others. A possible explanation for these discrepancies is that the OFES2 ocean model is not synchronised with observed data. However, the further work will need to be done to determine the precise cause.

IV. ESTIMATION OF THE QUALITY FACTOR OF THE CW

IV.I. Introduction

The Chandler period (*P*) and its quality factor (*Q*) are unique geophysical parameters that depend on the Earth's global dynamic response properties as a function of Earth's flattening, elastic and anelastic deformation and core-mantle decoupling (e.g., Smith and Dahlen 1981). The uniqueness of the *P* and *Q* also resides in their time scale that can bridge the seismological high-frequency band (1s – 54 min) with much lower frequencies, such as the 18.6-year, and even longer periods (e.g., Smith and Dahlen 1981; Benjamin et al. 2006; Lau and Faul 2019). Precision estimates of *P* and *Q* should also be beneficial for long-term prediction of polar motion. A plethora of prior estimates of *P* and *Q* been documented (e.g., Wilson and Vicente 1990; Furuya and Chao 1996; Seitz et al. 2012; Nastula and Gross 2015). However, substantial uncertainties persist in the estimation of *Q*, with range estimates from 49 to 179 (Bizoard 2020).

In recent study, Chen et al. (2023) sought to estimate *P* and *Q* without relying on geophysical excitation data, instead basing solely on observed polar motion data. However, adhering to the causality principle, one must either employ quality geophysical excitation data or at least assume any excitation process models, so we can reliably estimate *P* and *Q*. The first purpose of this chapter is to point out that we cannot optimise *P* and *Q* if we follow the approach by Chen et al. (2023). By replicating the result by Chen et al. (2023), we demonstrate that the cancellation of significant digits has led to their "optimum" estimates.

Meanwhile, Yamaguchi and Furuya (2024) proposed that the upper bound of *Q* could be constrained without geophysical excitation data, leveraging the recently observed CW anomaly. However, through our replication of the result by Chen et al. (2023), we have realised that it is not possible to constrain both *P* and *Q* solely from the observed polar motion data, even in the absence of CW. Consequently, we have decided to retract a portion of the claims made in Yamaguchi and Furuya (2024). However, Yamaguchi and Furuya (2024) also examined if the available and newly computed geophysical excitation data could explain the recently observed absence of CW and concluded that *Q* is not as high as 100, which we do not modify.

While we cannot formally exclude the possibility of temporal reduction in *Q* and/or alterations in *P* to explain the absence of the CW, no compelling geophysical evidence has been put forward to substantiate this hypothesis. In this chapter, we have adopted the assumption that both *P* and *Q* remain constant over time.

IV.II. Theory and Methodologies

As described in Chapter I.III., polar motion is governed by the following differential equation (Gross 2015),

$$\frac{i}{\tilde{\sigma}_{\mathrm{CW}}}\frac{d\tilde{p}}{dt}+\tilde{p}=\tilde{\chi}, \qquad (4-1)$$

where $\tilde{\sigma}_{\mathrm{CW}}$ is the complex Chandler frequency with its period (*P*) and *Q*:

$$\tilde{\sigma}_{\mathrm{CW}}\equiv\frac{2\pi}{P}\left(1+i\frac{1}{2Q}\right). \qquad (4-2)$$

The expressions with complex number for the celestial intermediate pole position (Gross 1992), $\tilde{p}(t)\equiv x(t)-iy(t)$, and the excitation, $\tilde{\chi}(t)\equiv\chi_1(t)+i\chi_2(t)$, allow us to analyse the 2D data with a first-order differential equation. Here, the $x(t)$ and $y(t)$ represent the location of the Pole along the Greenwich meridian and the 90°West Longitude, respectively, while the functions, denoted by $\chi_1(t)$

and $\chi_2(t)$ are referred to excitation functions and represent angular momentum around the two angular the two equatorial axes. A general solution of Eq. (4-1) consists of the following two terms:

$$\tilde{p}(t) = \tilde{p}_0 e^{i\tilde{\sigma}_{\mathrm{cw}}(t-t_0)} - i\tilde{\sigma}_{\mathrm{cw}} \int_{t_0}^{t} e^{i\tilde{\sigma}_{\mathrm{cw}}(t-\tau)} \tilde{\chi}(\tau) d\tau, \qquad (4-3)$$

which is essentially the same as Eqs. (2, 3, 4) in Chen et al. (2023); the subscript 0 indicates the initial value for each variable.

To examine if any geophysical sources can explain the observed polar motion, it has been conventional to first deconvolve the observed polar motion data into the "observed" (geodetic) excitation function ($\tilde{\chi}_{\mathrm{obs}}$), assuming *P* and *Q*, and next to compare with geophysical excitation function ($\tilde{\chi}_{\mathrm{geoph}}$) that is independent from the polar motion data. As long as the CW has been excited, namely, when the second term of right-hand side (RHS) of Eq. (4-3) is significant, minimising the misfit residuals between $\tilde{\chi}_{\mathrm{obs}}$ and $\tilde{\chi}_{\mathrm{geoph}}$ will tell the optimum estimates of *P* and *Q*. Therefore, reliable estimation of *P* and *Q* remains elusive until the available $\tilde{\chi}_{\mathrm{geoph}}$ sufficiently aligns with the $\tilde{\chi}_{\mathrm{obs}}$ based on the assumed *P* and *Q*; errors in the geophysical excitation data will control the uncertainties in the estimates, while those of space geodetic polar motion data are supposed to be now much smaller. Consequently, the estimation of *P* and *Q* and examination of the excitation sources have been tackled simultaneously, although those two themes have been separately published in the previous literature (e.g., Furuya et al. 1996, 1997; Furuya and Chao 1996). When global geophysical excitation data were unavailable, they used to make some assumptions such as "minimum excitation principle" (e.g., Wilson and Vicente 1990) and/or Gaussian random noise (e.g., Okubo 1982; Chao 1985).

As the Earth's dynamical response properties govern the values of *P* and *Q* (e.g., Smith and Dahlen 1981), they should also be taken into account in the $\tilde{\chi}_{\mathrm{geoph}}$. Instead of P and Q in the $\tilde{\chi}_{\mathrm{geoph}}$, numerical factors have to be multiplied to the mass and motion terms, respectively, in the $\tilde{\chi}_{\mathrm{geoph}}$ (e.g., Barnes et al. 1983; Wahr 1982; Gross 2015); the angular momentum of geofluids consists of both the moment of inertia term and the relative velocity term with respect to the rotating coordinate system, and each term is called the mass and motion term, respectively. The classical factors for the mass and motion terms were 1.00 and 1.43, respectively, because the observed *P* was 1.43 times the *P* of the rigid Earth and the factor for the mass term was reduced by 70% to 1.00 with the elastic load Love number, -0.3 (e.g., Munk and MacDonald 1960); those factors were subsequently modified to account for the core-mantle decoupling (Wahr 1982). Chen et al. (2023) designated these factors "transfer functions" and posited that they should in fact be complex numbers, thereby ensuring consistency with the complex Chandler frequency. We concur with the assertion; however, it should be noted that the imaginary part will diminish to an extent far less significant than the real part, even when *Q* is as low as 50. Consequently, for the sake of simplicity, we may discard the imaginary part in the transfer functions.

IV.III. Results and Discussion

Replication of Chen et al. (2023)'s result

In contrast to the forementioned standard approach, Chen et al. (2023) claimed that "only the observed polar motion data are needed" to estimate P and Q. In this study, we summarise and reiterate the approach by Chen et al. (2023) so that we can replicate their result.

First, the observed polar motion data are separated into the free-damping term and the excited polar motion term as indicated on the RHS of Eq. (4-3). The procedure for separating these two terms is outlined in the Appendix of Chen et al. (2023). To derive the excited polar motion term, we need to know the $\tilde{\chi}(\tau)$ in the second term of Eq. (4-3). Chen et al. (2023) state that "it is sufficient to use $\tilde{\chi}_{\mathrm{obs}}$ rather than $\tilde{\chi}_{\mathrm{geo}}$ here since this study does not discuss which geoprocess(es) contribute(s) the most to the excitations of CW". After computing the second term in the RHS of Eq. (4-3) under the assumption of *P* and *Q*, the free-damping term is derived by subtracting the computed excited polar motion from the observed polar motion; the free-damping term thus evidently depends on the assumed *P* and *Q* as well.

It is important to note that the decomposition into the free-damping and excited terms can be performed with any arbitrary pairs of *P* and *Q*. If the two terms are summed, the original polar motion data can always be reconstructed, regardless of the assumed *P* and *Q*. Two examples of this decomposition are shown in Figure 4-1: one into the free-damping term and excited polar motion term. Their combinations are also displayed, with the assumed pairs of *P* and *Q* are 300 days and 500 (Figure 4-1a) and 500 days and 30 (Figure 4-1c), respectively. The blue and red curves in Figures 4-1a and 4-1c represent the free-damping term and the excited polar motion term, respectively. The polar motion data used in this study is EOP 14 C04 from IERS (Bizouard et al. 2019), covering the period from 1962 to 2023. The recovered polar motion data in Figures 4-1b and 4-1d are precisely congruent. Namely, the polar motion data can be decomposed into the two distinct terms, with any arbitrary pairs of *P* and *Q*. This indicates that there are no criteria to pick up the optimum *P* and *Q* solely from the polar motion data. To derive the optimal *P* and *Q*, additional data and/or assumptions regarding the excitation processes are necessary.

Chen et al. (2023) introduced a single parameter D_{CW} defined as the product PQ, which is mathematically $-\pi$ divided by the slope of a natural logarithm of the free-damping term (Eq. 9 in Chen et al. 2023). Subsequently, Chen et al. (2023) "estimated" $\bar{D}_{\mathrm{CW}}$ from the calculated free-damping term. Theoretically, however, the estimated $\bar{D}_{\mathrm{CW}}$ should be strictly identical to the prescribed product PQ regardless of their values. Namely, the differences, $v \equiv \bar{D}_{CW} - PQ$, should always be zero in theory. Nevertheless, Chen et al. (2023) computed v for a range of pairs of P and Q, and identified the pairs that yielded the minimum v as optimal.

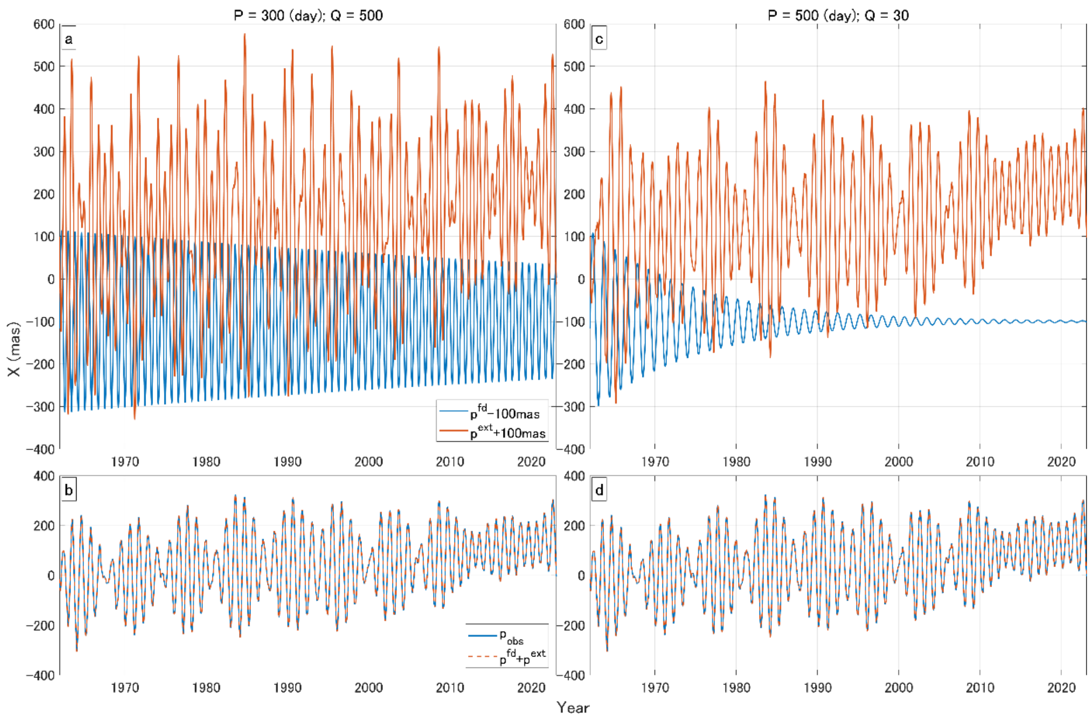

[Figure 4-1] (a) p^{fd} (blue) and p^{ext} (red) and (b) p_{obs} (blue) and $p^{fd}+p^{ext}$ (red-dashed) when P is 300 days and Q is 500. (c) p^{fd} (blue) and p^{ext} (red), and (d) p_{obs} (blue) and $p^{fd}+p^{ext}$ (red-dashed) when P is 500 days and Q is 30.

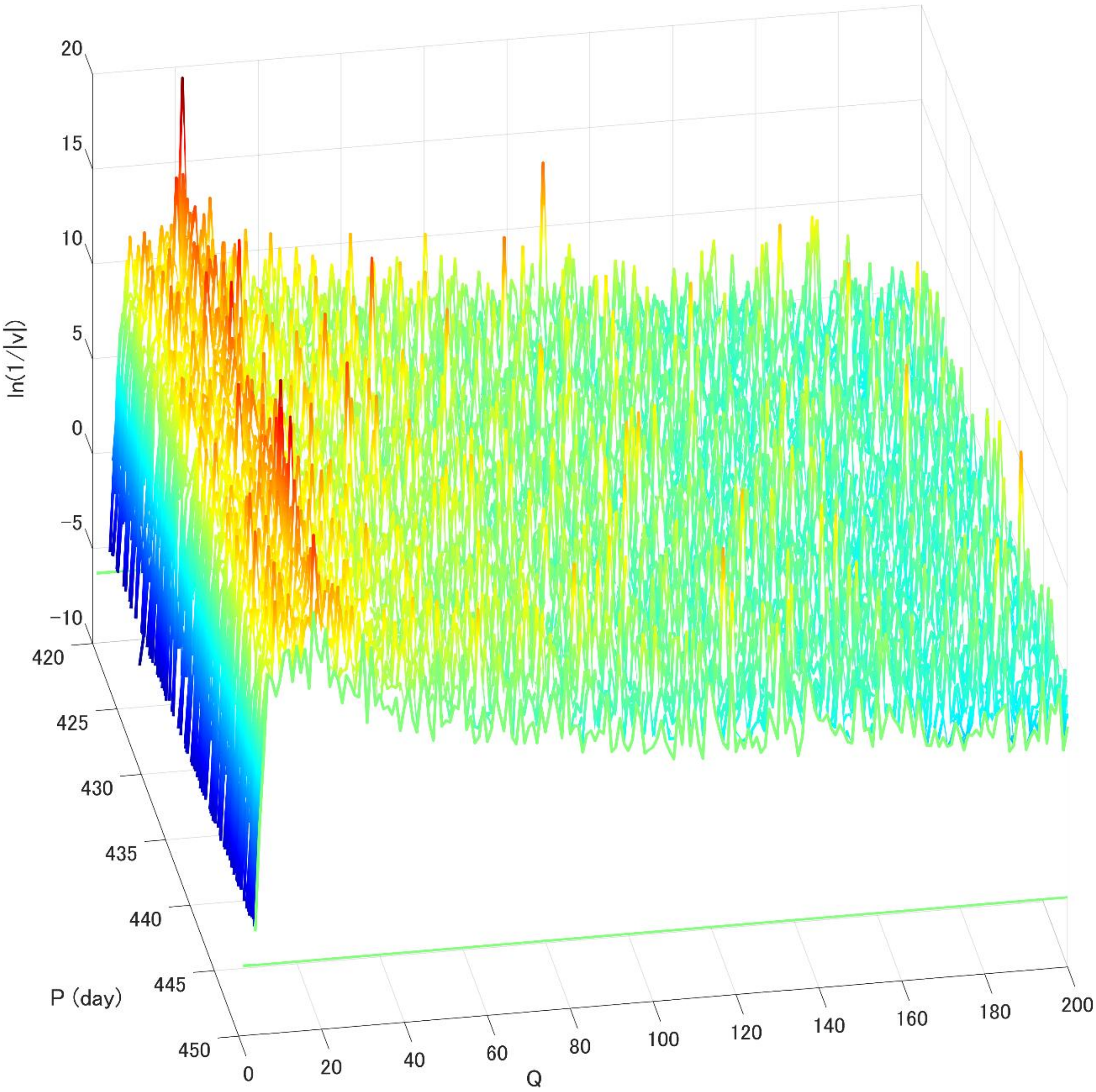

[Figure 4-2] Replication of Figure 5 in Chen et al. (2023). See main text for details

Given the requirement that $\overline{D}_{\mathrm{CW}}$ should be an exact match to the initial assumed D_{CW} ($\equiv PQ$), the numerically computed v will always take a negligibly small value. To replicate the result of Chen et al. (2023), we also computed the difference v and plotted the natural logarithm of $(1/|v|)$ as a function of P and Q in Figure 4-2. We expanded the range of Q to include lower values below 20, and examined the P and Q, ranging from 420 to 450 days for P and from 5 to 200 for Q, respectively. Figure 4-2 also displays multiple local extremes, as observed Chen et al. (2023) in Figure 5.

Figure 4-2 indicates noteworthy changes in ln(1/ $|v|$) that necessitate further discussion. Most notably, there are spiky peaks in certain regions, i.e., very small $|v|$, as depicted Figure 5 in Chen et al. (2023). While Chen et al. (2023) identified the pair of P and Q that yielded the minimum $|v|$ as optimum, we consider that those very high ln(1/ $|v|$) are attributable to the cancellation of significant digits, a well-documented pitfall in numerical analysis (e.g., Wilkinson 1963). For instance, when the assumed pairs of P and Q are (432.5, 132) and (432.5, 133), the exact D_{CW} are 57,090.000000 and 57,522.500000, respectively. However, our numerical estimates of $\overline{D}_{CW}$ yielded 57,089.968867 and 57,522.499988, respectively, and the resulting $|v|$ became 0.031133 and 0.000012, respectively. The latter pair (432.5, 133) generates substantially smaller $|v|$, yet it cannot be considered "more optimum" than the former pair (432.5, 132). The numerous spiky peaks in Figure 4-2 are attributed to the cancellation of digits, and there are no physical reasons why those P and Q are generating the minimum $|v|$, namely, maximum ln(1/ $|v|$).

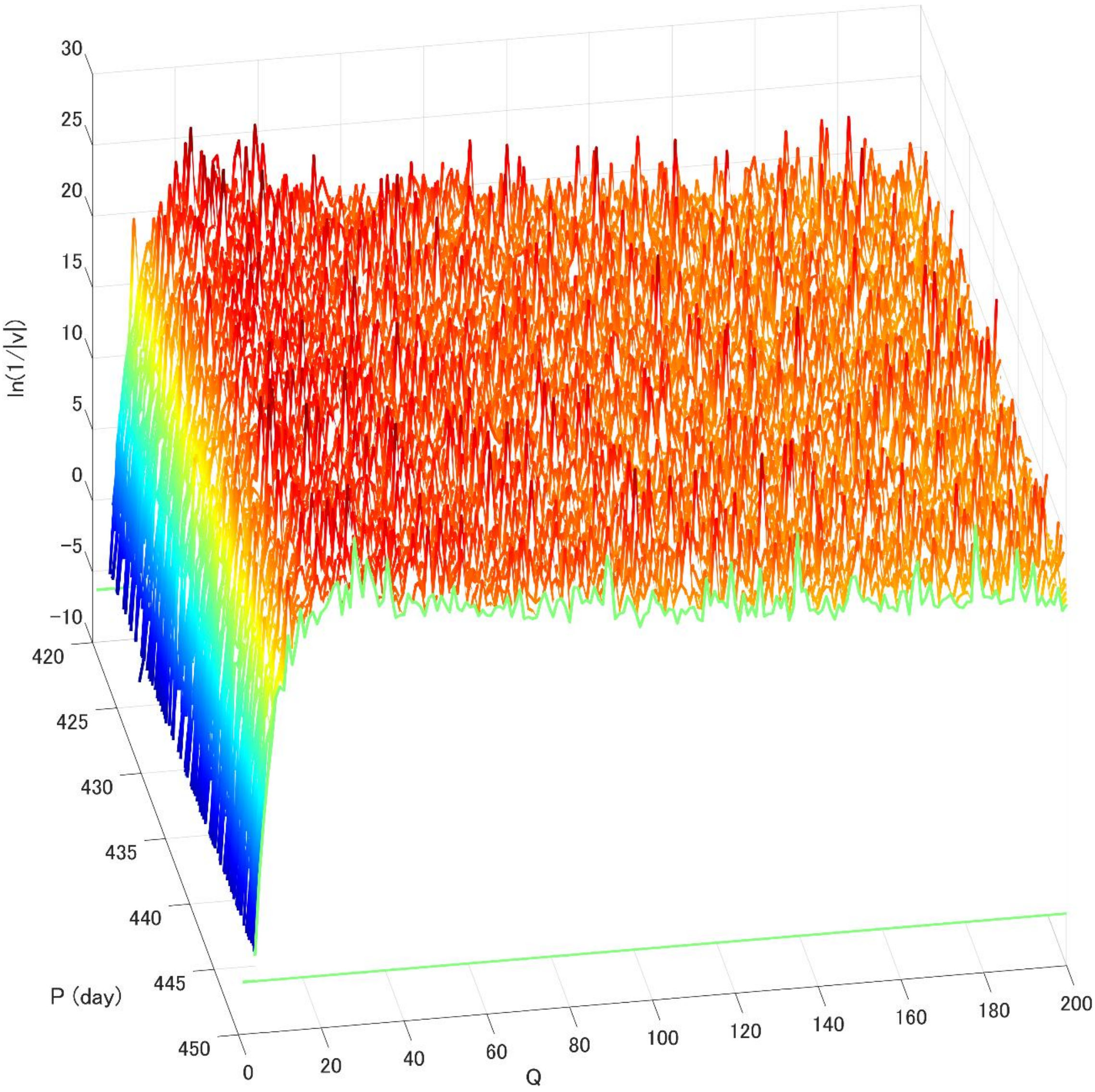

[Figure 4-3] Replication of the Figure 5 in Chen et al. (2023) using MATLAB "polyfit" command. See main text for details

The presence of numerical issues was revealed when an alternative algorithm was employed to estimate the slope of a natural logarithm of the free-damping term. Although Figure 4-2 was generated by the "lsqr" in MATLAB to estimate the aforementioned slope, an alternative result was derived and presented in Figure 4-3 that used "polyfit" function in MATLAB. When the assumed pairs of *P* and

Q are (432, 50), the exact D_{CW} is 21600. However, the numerical estimates of $\overline{D}_{\mathrm{CW}}$ became 21600.0028134440 by “lsqr” and 21599.9999999846 by “polyfit”, and the resulting $\ln(1/|\nu|)$ were 5.87334593 and 17.98727431, respectively. The significant discrepancy in these results is again attributed to the cancellation of the significant digits.

The limitation of an alternative simple application constraining *P* and *Q*

Yamaguchi and Furuya (2024) proposed “A simple approach to constrain the upper bound of *Q*”, taking advantage of the recent diminishment of the 6-year beat in the polar motion data. However, we here retract the assertion in Yamaguchi and Furuya (2024) that “we can take advantage of the recent CW anomaly to more tightly constrain the upper bound of *Q* of the CW” because the analysis was lacking careful considerations on the free-damping CW by the initial values. We demonstrate below that the proposed simple approach, based exclusively on the polar motion data, is inadequate in constraining both *P* and *Q*. Nonetheless, we maintain our position that higher *Q* (>100) and lower *Q* (<25) are improbable, as substantiated by the atmospheric, oceanic, and hydrological contributions examined by Yamaguchi and Furuya (2024).

Yamaguchi and Furuya (2024) compared two different CW time-series data. The first one is what we call the observed Chandler wobble ($\mathrm{CW_{obs}}$), which can be simply derived by removing the AW (Figures 4-4a, b) in this chapter and Figure 4 in Yamaguchi and Furuya (2024) without assuming the *P* and *Q*. From 2015 to 2021, the 6-year beat by the AW and CW became apparently insignificant, meaning that only the AW was present (Figure 1 in Yamaguchi and Furuya 2024). The AW can be extracted by a simple least-squares method. The phase of the AW is constant by definition, as it is a forced motion driven by seasonal excitation, and the amplitude modulation is minor (Gross 2015). Therefore, once we estimate the amplitude and phase of the AW during the 2015-2021 period are estimated, the AW signal can be removed from the entire polar motion time series. In addition, the quadratic long-term motion is removed from the observed polar motion.

The second one is the estimated Chandler wobble (CW_{est}), derived from deconvolution and re-integration of observed polar motion data (Figures 4-4a, b). Yamaguchi and Furuya (2024) designated it the "geodetic CW", yet we designated the estimated CW (CW_{est}) in this chapter to avoid confusion with the CW_{obs}. We assume consistently the same *P* and *Q* for the deconvolution and re-integration to extract the CW_{est}. We must remove the seasonal signals from $\tilde{\chi}_{\mathrm{geod}}$ prior to the re-integration, and the initial value of the re-integration was set to be zero to avoid the effects of both a free-damping CW and transient CW term (Furuya et al. 1997; Yamaguchi and Furuya 2024). We discuss below, however, that we need to include the free-damping CW.

We further compute the third CW time series, which we denote as $CW_{obs\text{-}int}$ (Figures 4-4a, b). An additional excitation function is obtained by deconvolving CW_{obs} under the assumed values of *P* and *Q*. After removing the annual components using the least-squares method, $CW_{obs\text{-}int}$ is derived by re-integrating the excitation function with the same assumed *P* and *Q*. The differences between the CW_{est} and $CW_{obs\text{-}int}$ stem from the method of removing the seasonal signal and become apparent below, with consequences for the study of excitation sources, as we will address subsequently. Figure 4-5 shows the procedure to calculate three estimated CWs. Although the annual components of CW_{est} are removed from the excitation function after deconvolution, those of the $CW_{obs\text{-}int}$ are removed from the polar motion data before deconvolution.

A critical issue in the proposed "simple approach" by Yamaguchi and Furuya (2024) is the omission of the effect of the free-damping CW from the initial value on the recent misfit between the CW_{est} (and $CW_{obs\text{-}int}$) and CW_{obs}. It is true that the discrepancy between the CW_{obs} and CW_{est} in recent period after 2015 appears to be more pronounced in the larger *Q* (the lowermost curve in Figure 4 of

Yamaguchi and Furuya 2024), which seemingly corroborates the hypothesis that the higher Q would be implausible. However, the observed discrepancy can be straightforwardly ascribed to the free-damping CW that is derived by subtracting the CW_{est} (or $CW_{obs\text{-}int}$) from the CW_{obs}, as shown in Figures 4-4c, d.

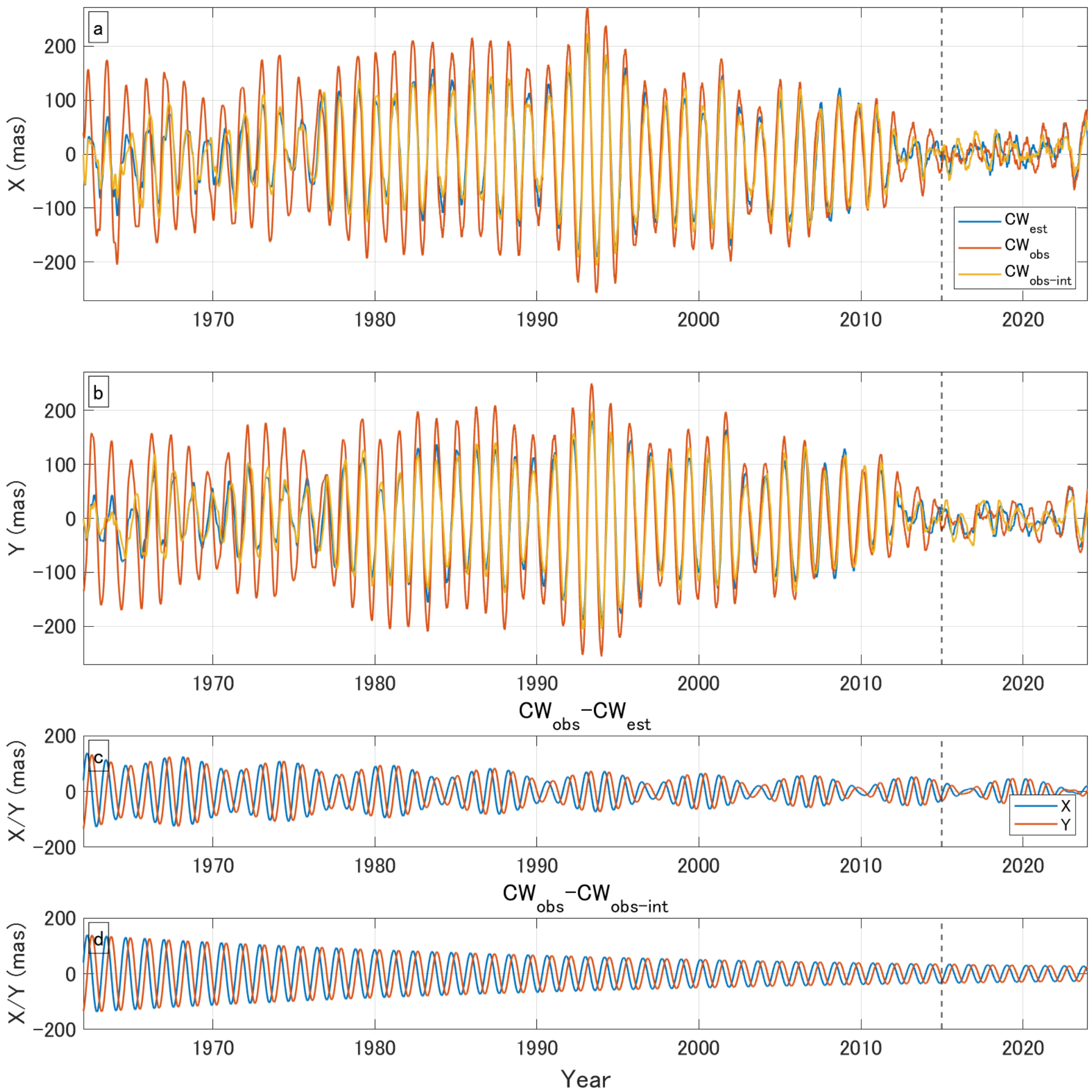

[Figure 4-4] (a)(b) X/Y component of CW_{est} (blue), CW_{obs} (red), and $CW_{obs\text{-}int}$ (yellow). (c) X (blue) and Y (red) components of the difference, CW_{obs} - CW_{est}. (d) X (blue) and Y (red) components of the difference, CW_{obs} - $CW_{obs\text{-}int}$.

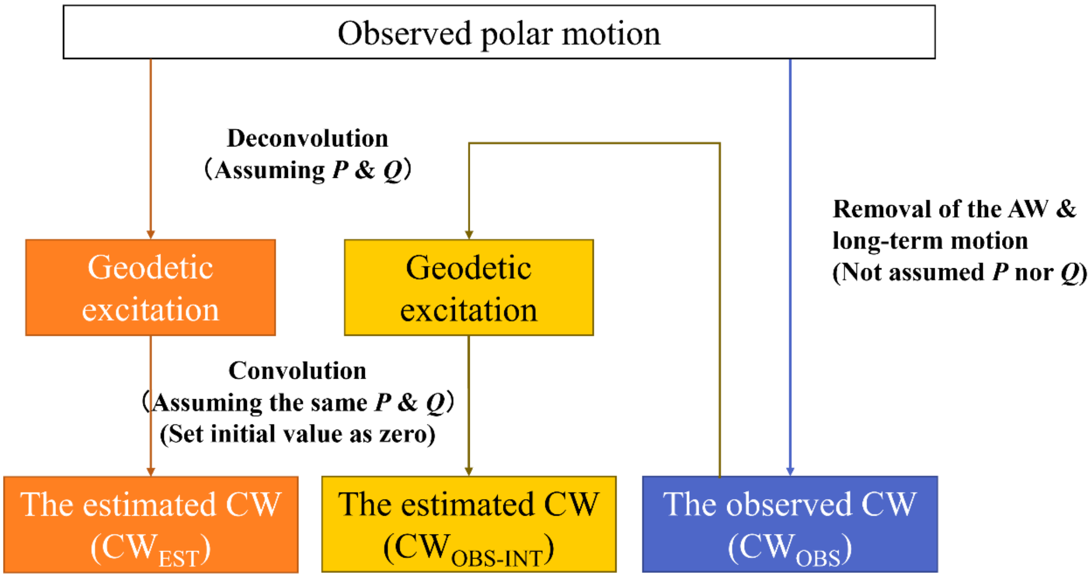

[Figure 4-5] Flowchart of an alternative approach for estimating *P* and *Q* using only the observed polar motion data.

To assess how CW_{est} and $CW_{obs\text{-}int}$ could match the CW_{obs}, Yamaguchi and Furuya (2024) defined the variance reduction (VR) metric as

$$\mathrm{VR} = 1 - \frac{\int_{t_0}^{t_1} \left|\left|\mathcal{O}(\tau) - \mathcal{C}(\tau)\right|\right|^2 \mathrm{d}\tau}{\int_{t_0}^{t_1} \left|\left|\mathcal{O}(\tau)\right|\right|^2 \mathrm{d}\tau}, \qquad (4-4)$$

where $C(t)$ and $O(t)$ are the calculated (CW_{est} and $CW_{obs\text{-}int}$) and observed data (CW_{obs}) that do and do not depend on the assumed *P* and *Q*, respectively. The closer the VR to 1, the better is the agreement between $O(t)$ and $C(t)$.

The Figure 4-6 shows a correction to Figure S5 of Yamaguchi and Furuya (2024). In Figure S5 of Yamaguchi and Furuya (2024), the effect of the free-damping CW was erroneously not considered in $C(t)$. Consequently, only the cases with lower Q generated the high VR close to 1, because the lower Q makes the free-damping CW more quickly diminish. However, when the free-damping CW is incorporated into the calculated $CW_{obs\text{-}int}$ (or CW_{est}) the VR invariably becomes identical to 1, irrespective of the assumed *P* and *Q*, as illustrated in Figure 4-5. This indicates that the *P* and *Q* cannot be optimised solely from the observed polar motion data. The actual deviations from 1.0 in Figure 4-5 are attributable numerical errors and are negligible.

While AW signals were removed from the original polar motion data to derive the CW_{obs}, the non-optimisability of *P* and *Q* based solely on the polar motion data is also evident from Figure 4-1.

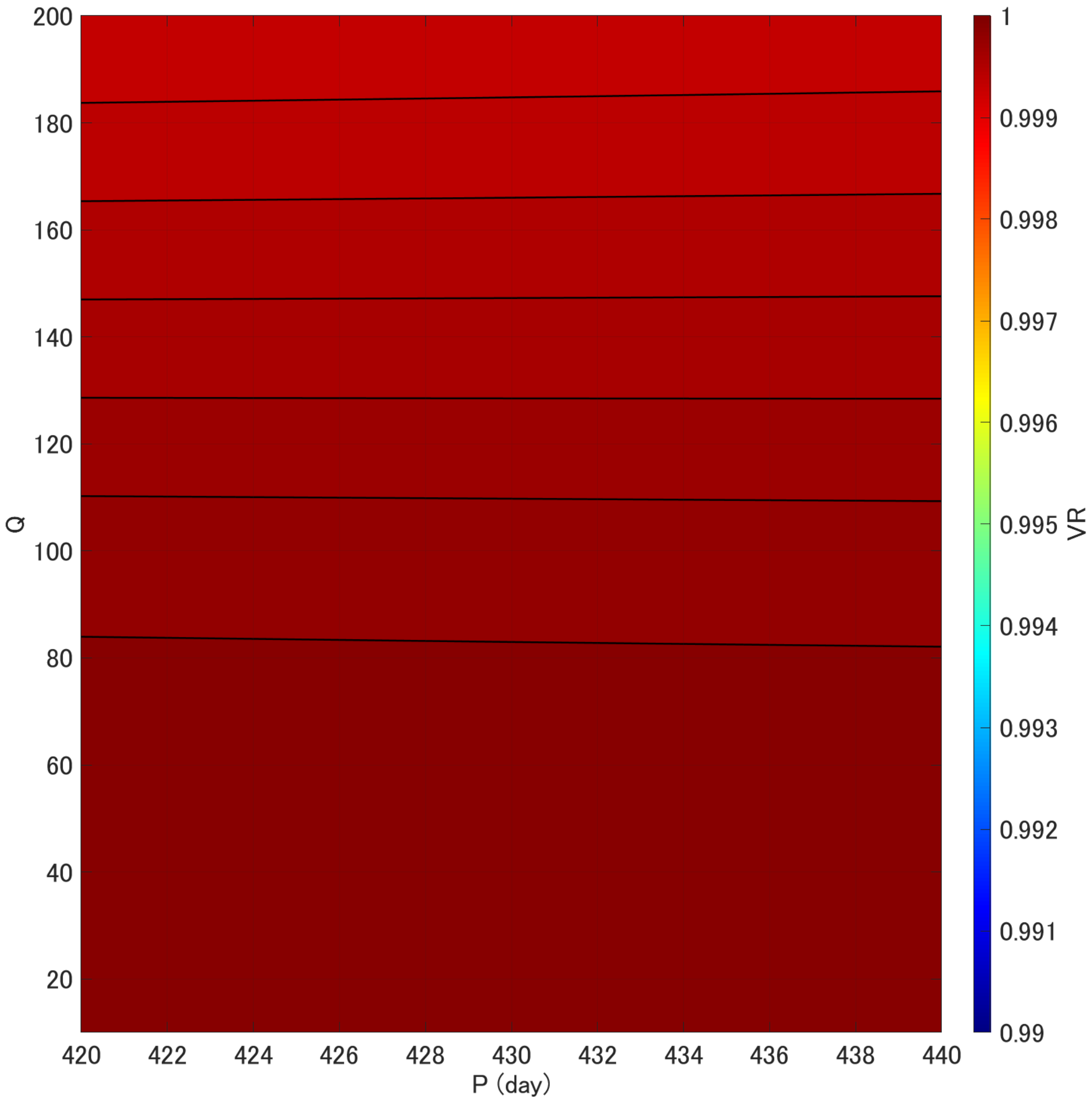

[Figure 4-6] Variance reduction (VR) map as a function of the assumed *P* and *Q* when the effect of the free damping term is added to the calculated CW. The VR is over 99.9% regardless of the assumed *P* and *Q* in this range.

Notably, the two residuals, i.e., $CW_{obs}-CW_{est}$ and $CW_{obs}-CW_{obs\text{-}int}$, depicted in Figure 4-4c, d, respectively, exhibit distinct characteristics. The former residual from CW_{est} displays a ~6-year beat, while the latter from $CW_{obs\text{-}int}$ does not (Figure 4-4). This observation signifies the presence of annual signals in CW_{est} attributable to the incomplete removal of annual signals from the deconvoluted geodetic excitation function. Consequently, numerous previously derived “non-seasonal” geodetic excitation functions have been found to encompass residual seasonal signals, thereby impeding a thorough examination of the CW excitation. The incomplete removal of annual signals can be attributed to the relatively noisy nature of the geodetic excitation function.

IV.IV. Summary

Recently, Chen et al. (2023) and Yamaguchi and Furuya (2024) have presented claims regarding the optimisation or constraint of *P* and *Q*, derived exclusively from the polar motion data. However, we pointed out the problems in the two papers. To ensure the reliability of *P* and *Q* estimates, it is essential to either utilise high-quality geophysical excitation data or employ models that are capable of simulating excitation processes. The accurate estimation of *Q* is of particular significance, as it not only improves our understanding of mantle anelasticity but also facilitates physics-based long-term predictions of polar motion.

While the well-known ~1.2-year Chandler period has been inferred from the clear ~6-year period of beat in the polar motion time-series, it is crucial to acknowledge that a model of random excitation with a flat power spectrum around the resonant frequency was assumed. The ~6-year beat has become apparently unclear in the recent polar motion data, which is unprecedented occurrence and thus may suggest a need to renew the conventional understanding of the polar motion.

If the excitation process of CW is truly random as often assumed, we would first speculate a “cancellation scenario” to account for the absence of CW in which atmosphere, ocean, and land hydrology are equally contributing with different phases and eventually cancelling each other. An observation by Yamaguchi and Furuya (2024) merits attention. The two independent AAM data from ERA5 and JRA-55 were found to be almost perfectly aligned with each other in terms of their persistently smaller contributions to the CW excitations in recent years. This suggests the possibility that the combined effects of ocean and land hydrology could be cancelling each other recently. However, the absence of quantitative evidence hinders the substantiation of this hypothesis. The availability of high-quality oceanic and hydrological angular momentum data is imperative to further advance our understanding of this phenomenon and possibly reveal non-random (near-resonant) excitation processes.

V. CONCLUSION

We have found that the CW was absent from 2015 to 2021 and set our purpose to clarify the mechanism of the excitation and damping of the CW.

In chapter II, we calculated the new AAM based on the atmospheric reanalysis data, JRA-55. In addition, we found that the atmospheric contribution to the excitation of the CW decreased in the same term as the absence of the CW.

In chapter III, we preliminarily calculated the OAM based on the OFES2 ocean model data. The combination of the OFES2 OAM and the JRA55 AAM will be the third set of the AAM and OAM in the world.

In chapter IV, we argue whether P and Q can be estimated by only the observed polar motion data taking advantage of the absence of the CW. Since the difference obtained by this method is below significance, it suggests that the excitation data must be needed for the estimation of P and Q.

In general, this study provides the major progress on the understanding of the excitation mechanism of the CW, which is long considered resolved. Our results have gone some way towards enhancing our understanding of the interaction between the atmosphere and ocean and the solid Earth, and the estimation of the Earth's internal structure.

AKNOWLEDGEMENT

I would like to thank the following people for their support, which is indispensable to my work.

Firstly, I gratefully acknowledge Prof. Masato FURUYA, who is my supervisor, for comprehensive support for my research. In addition, I would like to express my sincere gratitude to Prof. Masaru INATSU and Assoc. Prof. Youichiro TAKADA for their many valuable comments and constructive advice on this dissertation. Furthermore, I wish to thank Prof. Kosuke HEKI, Assoc. Prof. Youichiro TAKADA, Prof. Kiyoshi YOMOGIDA, Prof. Kazunori YOSHIZAWA, and Assoc. Prof. Makoto NAOI for constructive discussions and suggestions. Thanks are also due to all members of the solid Earth seminar for both academic and personal relationships.

I thank the following institutions which provide data used in my research. The JRA-55 data is provided by the Laboratory of Meteorology, Hokkaido University. The EOP data is provided by the International Earth Rotation and Reference Service (IERS). The NCEP AAM and ECCO OAM data are provided by Paris Observatory. And the ECMWF AAM, MPIOM OAM, and LSDM HAM data are provided by the Earth System Modelling Group of GeoForschungsZentrum Potsdam (ESMGFZ). The OFES ver.2 data are provided by the Japan Agency for Marne-Earth Science and Technology (JAMSTEC). Content of Chapter II has already been published as Yamaguchi and Furuya (2024), and content of Chapter IV has been published as Yamaguchi and Furuya (2025). Both papers were published in *Earth, Plantes and Space*.

I would also like to thank for my family for their understanding and financial support throughout my long academic career. The financial support was also given by JST SPRING, Grant Number JPMJSP2119 for four years of master's and doctoral programmes.

Last but not least, I appreciate all researchers who discussed or reviewed my work.

BIBLIOGRAPHY

Anstey JA, Banyard TP, Butchart N, Coy L, Newman PA, Osprey S, Wright CJ (2021) Prospect of increased disruption to the QBO in a changing climate. Geophys Res Lett 48:e2021GL093058. https://doi.org/10.1029/2021GL093058

Aoyama Y, Naito I (2001) Atmospheric excitation of the Chandler wobble, 1983–1998. J Geophys Res Solid Earth 106(B5):8941–8954. https://doi.org/10.1029/2000JB900460

Aoyama Y, Naito I, Iwabuchi T, Yamazaki N (2003) Atmospheric quasi-14 month fluctuation and excitation of the Chandler wobble. Earth Planets Space 55(12):e25 – e28. https://doi.org/10.1186/BF03352480

Baldwin MP, Gray LJ, Dunkerton TJ, Hamilton K, Haynes PH, Randel WJ, Holton JR, Alexander MJ, Hirota I, Horinouchi T, Jones DBA, Kinnersley JS, Marquardt C, Sato K, Takahashi M (2001) The quasi-biennial oscillation. Rev Geophys 39(2):179–229. https://doi.org/10.1029/1999RG000073

Barnes RTH, Hide R, White AA, Wilson CA (1983) Atmospheric angular momentum fluctuations, length-of-day changes and polar motion. Proc R Soc Lond A 387:31 – 73. https://doi.org/10.1098/rspa.1983.0050

Benjamin D, Wahr J, Ray RD, Egbert GD, Desai SD (2006) Constraints on mantle anelasticity from geodetic observations, and implications for the J2 anomaly. Geophys J Int 165:3 – 16. https://doi.org/10.1111/j.1365-246X.2006.02915.x

Bizouard C (2020) Geophysical modelling of the polar motion. De Gruyter, Berlin

Bizouard C, Lambert S, Gattano C, Becker O, Richard JY (2019) The IERS EOP 14C04 solution for Earth orientation parameters consistent with ITRF 2014. J Geodesy 93:621–633. https://doi.org/10.1007/s00190-018-1186-3

Börger L, Schindelegger M, Zhao M, Ponte RM, Löcher A, Uebbing B, Molines JM, Penduff T (2025) Chaotic oceanic excitation of low-frequency polar motion variability. Earth Syst Dynam 16:75-90. https://doi.org/10.5194/esd-16-75-2025

Brzeziński A, Nastula J (2002) Oceanic excitation of the Chandler wobble. Adv Space Res 30(2):195–200. https://doi.org/10.1016/S0273-1177(02)00284-3

Chao BF (1985) On the Excitation of the Earth's polar motion. Geophys Res Lett 12(8):526–529. https://doi.org/10.1029/GL012i008p00526

Chao BF (1989) Length-of-day variations caused by El Niño-southern oscillation and quasi-biennial oscillation. Science 243:4893. https://doi.org/10.1126/science.243.4893.923

Chao BF, Chung WY (2012) Amplitude and phase variations of Earth's Chandler wobble under continual excitation. J Geodyn 62:35–39. https://doi.org/10.1016/j.jog.2011.11.009

Chen JL, Wilson CR, Ries JC, Tapley BD (2013) Rapid ice melting drives Earth's pole to the east. Geophys Res Lett 40:2625–2630. https://doi.org/10.1002/grl.50552

Chen W, Chen Y, Ray J, Luo J, Cheng Li J (2023) Free decay and excitation of the chandler wobble: self-consistent estimates of the period and quality factor. J Geodesy 97:36. https://doi.org/10.1007/s00190-023-01727-z

Dahlen FA (1973) A correction to the excitation of the Chandler wobble by earthquakes. Geophys J R Astron Soc 32:203–217. https://doi.org/10.1111/j.1365-246X.1973.tb06527.x

Dee DP, Uppala SM, Simmons AJ, Berrisford P, Poli P, Kobayashi S, Andrae U, Balmaseda MA, Balsamo G, Bauer P, Bechtold P, Beljaars ACM, van de Berg L, Bidlot J, Bormann N, Delsol C, Dragani R, Fuentes M, Geer AJ, Haimberger L, Healy SB, Hersbach H, Hólm EV, Isaksen L, Kållberg P, Köhler M, Matricardi M, McNally AP, Monge-Sanz BM, Morcrette JJ, Park BK, Peubey C, de Rosnay P, Tavolato C, Thépaut JN, Vitart F (2011) The ERA-Interim reanalysis: configuration and performance of the data assimilation system. Q J R Meteorol Soc 137: 553-597. https://doi.org/10.1002/qj.828

Dill R (2008) Hydrological model LSDM for operational Earth rotation and gravity field variations. Deutsches GeoForschungsZentrum GFZ, Potsdam

Ding H, Chao BF (2017) Solid pole tide in global GPS and superconducting gravimeter observations: Signal retrieval and inference for mantle anelasticity. Earth and Planetary Sci Lett 459:244-251. https://doi.org/10.1016/j.epsl.2016.11.039

Dobslaw H, Dill R (2017) Predicting Earth orientation changes from global forecasts of atmosphere-hydrosphere dynamics. Adv Space Res 61(2018):1047-1054. https://doi.org/10.1016/j.asr.2017.11.044

Dobslaw H, Dill R, Grötzsch A, Brzeziński A, Thomas M (2010) Seasonal polar motion excitation from numerical models of atmosphere, ocean, and continental hydrosphere. J Geophys Res 115:B10406. https://doi.org/10.1029/2009JB007127

ECCO Consortium, Fukumori I, Wang O, Fenty I, Forget G, Heimbach P, Ponte RM (2021) ECCO ocean bottom pressure – Monthly mean 0.5 degree (Version 4 Release 4 B). Ver.V4r4b. PO.DAAC, CA, USA. Dataset accessed [2025-04-30]. https://doi.org/10.5067/ECG5M-OBP4B

Eubanks T, Steppe J, Dickey J, Rosen R, Salstein D (1988) Causes of rapid motions of the Earth's pole. Nature 334:115–119. https://doi.org/10.1038/334115a0

Forget G, Campin JM, Heimbach P, Hill CN, Ponte RM, Wunsch C (2015) ECCO version 4: an integrated framework for non-linear inverse modeling and global ocean state estimation, Geosci Model Dev 8:3071–3104, https://doi.org/10.5194/gmd-8-3071-2015

Furuya M, Hamano Y, Naito I (1996) Quasi-periodic wind signal as a possible excitation of Chandler wobble. J Geophys Res 101(B11):25537–25546. https://doi.org/10.1029/96JB02650

Furuya M, Chao BF (1996) Estimation of period and Q of the Chandler wobble. Geophys J Int 127(3):693–702. https://doi.org/10.1111/j.1365-246X.1996.tb04047.x

Furuya M, Hamano Y, Naito I (1997) Importance of wind for the excitation of Chandler wobble as inferred from wobble domain analysis. J Phys Earth 45(3):177–188. https://doi.org/10.4294/jpe1952.45.177

Greatbatch RJ (1994) A note on the representation of steric sea level in models that conserve volume rather than mass. J Geoph Res 99(C6):12767-12771. https://doi.org/10.1029/94JC00847

Gross RS (1992) Correspondence between theory and observations of polar motion. Geophys J Int 109:162–170. https://doi.org/10.1111/j.1365-246X.1992.tb00086.x

Gross RS (2015) Earth rotation variations-long period. In: Schubert G (ed) Treatise in Geophysics, vol 3, 2nd edn. Elsevier, pp 215–261

Gross RS (2000) The excitation of the Chandler wobble. Geophys Res Lett 27(15):2329–2332. https://doi.org/10.1029/2000GL011450

Gross RS, Fukumori I, Menemenlis D (2003) Atmospheric and oceanic excitation of the Earth's wobbles during 1980–2000. J Geophys Res 108(B8):2370. https://doi.org/10.1029/2002JB002143

Gross RS (2015) Earth rotation variations-long period. In: Schubert G (ed) Treatise in Geophysics, 2nd edn. Amsterdam, Elsevier

IOC, SCOR, IAPSO (2010) The international thermodynamic equation of seawater - 2010: Calculation and use of thermodynamic properties. Intergovernmental Oceanographic Commission, Manuals and Guides No. 56, UNESCO (English) pp 196.

JAMSTEC (2009) JAMSTEC OFES (Ocean General Circulation Model for the Earth Simulator) Dataset, JAMSTEC. https://doi.org/10.17596/0002029

Jungclaus JH, Fischer N, Haak H, Lohmann K, Marotzke J, Matei D, Mikolajewicz U, Notz D, vonStorch JS (2013) Characteristics of the ocean simulations in MPIOM, the ocean component of the MPI-Earth system model, J Adv Model Earth Syst, 5:422–446. https://doi.org/10.1002/jame.20023

Kalnay E, Kanamitsu M, Kistler R, Collins W, Deaven D, Gandin L, Iredell M, Saha S, White G, Woollen J, Zhu Y, Chelliah M, Ebisuzaki W, Higgins W, Janowiak J, Mo KC, Ropelewski C, Wang J, Leetmaa A, Reynolds R, Jenne R, Joseph D (1996) The NCEP/NCAR 40-Year Reanalysis Project. Bull Am Meteorol Soci 77(3): 437-472. https://doi.org/10.1175/1520-0477(1996)077<0437:TNYRP>2.0.CO;2

Kobayashi S, Ota Y, Harada Y, Ebita A, Moriya M, Onoda H, Onogi K, Kamahori H, Kobayashi C, Endo H, Miyaoka K, Takahashi K (2015) The JRA-55 reanalysis: general specifications and basic characteristics. J Meteorol Soc Jpn 93:5–48. https://doi.org/10.2151/jmsj.2015-001

Lau HCP, Faul UH (2019) Anelasticity from seismic to tidal timescales: theory and observations. Earth Planet Sci Lett 508:18–29. https://doi.org/10.1016/j.epsl.2018.12.009

Malkin Z, Miller N (2010) Chandler wobble: two more phase jumps revealed. Earth Planets Space 62:943–947. https://doi.org/10.5047/eps.2010.11.002

McDougall TJ, Barker PM (2011) Getting started with TEOS-10 and the Gibbs Seawater (GSW) oceanographic toolbox, SCOR/IAPSO WG127, pp 28.

Munk WH, MacDonald GJF (1960) The rotation of the Earth: a geophysical discussion. Cambridge University Press, New York

Nastula J, Gross R (2015) Chandler wobble parameters from SLR and GRACE. J Geophys Res Solid Earth 120:4474–4483. https://doi.org/10.1002/2014JB011825

National Centers for Environmental Prediction, National Weather Service, NOAA, U.S. Department of Commerce. (1994). NCEP/NCAR Global Reanalysis Products, 1948-continuing. NSF National Center for Atmospheric Research. https://gdex.ucar.edu/datasets/d090000

Newman PA, Coy L, Pawson S, Lait LR (2016) The anomalous change in the QBO in 2015–2016. Geophys Res Lett 43:8791–8797. https://doi.org/10.1002/2016GL070373

Okubo S (1982) Is the Chandler period variable? Geophys J R Astron Soc 71(3):629–646. https://doi.org/10.1111/j.1365-246X.1982.tb02789.x

Ooe M (1978) An optimal complex AR.MA model of the Chandler wobble Geophys J Int 53(3):445-457. https://doi.org/10.1111/j.1365-246X.1978.tb03752.x

Osprey SM, Butchart N, Knight JR, Scaife AA, Hamilton K, Anstey JA, Schenzinger V, Zhang C (2016) An unexpected disruption of the atmospheric quasi-biennial oscillation. Science 353:6306. https://doi.org/10.1126/science.aah4156

Ponte R, Stammer D, Marshall J (1998) Oceanic signals in observed motions of the Earth's pole of rotation. Nature 391:476‐479. https://doi.org/10.1038/35126

Plag HP (1997) Chandler wobble and pole tide in relation to interannual atmosphere-ocean dynamics. In: Wilhelm H, Zürn W, Wenzel H-G (eds) Tidal Phenomena Lecture Notes in Earth Sciences. Springer, Heidelberg, pp 183‐218

Quinn KJ, Ponte RM, Heimbach P, Fukumori I, Campin JM (2019) Ocean angular momentum from a recent global state estimate, with assessment of uncertainties. Geophys J Int 216:584-597 https://doi.org/10.1093/gji/ggy452

Salstein DA, Kann DM, Miller AJ, Rosen RD (1993). The Sub-bureau for Atmospheric Angular Momentum of the International Earth Rotation Service: A Meteorological Data Center with Geodetic Applications. Bull Am Meteorol Soci 74(1):67-80. https://doi.org/10.1175/1520-0477(1993)074<0067:TSBFAA>2.0.CO;2

Sasaki H, Kida S, Furue R, Aiki H, Komori N, Masumoto Y, Miyama T, Nonaka M, Sasai Y, Taguchi B (2020) A global eddying hindcast ocean simulation with OFES2. Geoschi Model Dev Discuss 13:3319-3336 https://doi.org/10.5194/gmd-13-3319-2020

Seitz F, Kirschner S, Neubersch D (2012) Determination of the Earth's pole tide Love number k2 from observations of polar motion using an adaptive Kalman filter approach. J Geophys Res Solid Earth 117:B09403. https://doi.org/10.1029/2012JB009296

Seitz F, Schmidt M (2005) Atmospheric and oceanic contributions to Chandler wobble excitation determined by wavelet filtering. J Geophys Res 110:B11406. https://doi.org/10.1029/2005JB003826

Seitz F, Kirschner S, Neubersch D (2012) Determination of the Earth’s pole tide Love number k2 from observations of polar motion using an adaptive Kalman filter approach. J Geophys Res Solid Earth 117:B09403. https://doi.org/10.1029/2012JB009296

Smith ML, Dahlen FA (1981) The period and Q of the Chandler wobble. Geophys J R Astron Soc 64:223–281. https://doi.org/10.1111/j.1365-246X.1981.tb02667.x

Vondrák J, Ron C (2005) The great Chandler wobble change in 1923–1940 re-visited. In: Plag HP, Chao BF, Gross RS, van Dam T (eds) Forcing of Polar Motion in the Chandler Frequency Band: A Contribution to Understanding Interannual Climate Change. Cahiers du Centre Européen de Géodynamique et de Séismologie, Luxembourg, pp 39–42

Wahr JM (1982) The effects of the atmosphere and oceans on the Earth’s wobble−I. Theory. Geophys J Roy Astron Soc 70:349–372. https://doi.org/10.1111/j.1365-246X.1982.tb04972.x

Wang S, Wilson CR, Chen J, Seo K, Fu Y, Kuang W (2025) Variability of annual polar motion and its relationship to the Chandler wobble. Proc Natl Acad Sci U.S.A 122(48) e2520272122. https://doi.org/10.1073/pnas.2520272122

Wilkinson JH (1963) Rounding errors in algebraic processes. Her Majesty’s Stationary Office, London

Wilson CR, Haubrich RA (1976) Meteorological excitation of the Earth’s wobble Geophys J I 46(3):707-743. https://doi.org/10.1111/j.1365-246X.1976.tb01254.x

Wilson CR, Vicente RO (1990) Maximum likelihood estimates of polar motion parameters. In: McCarthy DD, Carter WE (eds) Variations in Earth Rotation, Geophysical Monograph Series. American Geophysical Union, Washington, pp 151–155

Wilson CR (1985) Discrete polar motion equations. Geophys J R Astron Soc 80:551–554. https://doi.org/10.1111/j.1365-246X.1985.tb05109.x

Xu XQ, Fang M, Zhou YH, Liao XH (2024) Continental and oceanic AAM contributions to Chandler wobble with the amplitude attenuation from 2012 to 2022. J Geod 98:59. https://doi.org/10.1007/s00190-024-01872-z

Yamaguchi R, Furuya M (2024) Can we explain the post-2015 absence of the Chandler wobble? Earth Planets Space 76:1. https://doi.org/10.1186/s40623-023-01944-y

Yamaguchi R, Furuya M (2025) Can we estimate the period and quality-factor of the Chandler wobble using only the observed polar motion data?. Earth Planets Space 77:99. https://doi.org/10.1186/s40623-025-02240-7

Zotov L, Bizouard C, Shum CK, Zhang C, Sidorenkov N, Yushkin V (2022) Analysis of Earth's polar motion and length of day trends in comparison with estimates using second degree stokes coefficients from satellite gravimetry. Adv Space Res 69(1):308–318. https://doi.org/10.1016/j.asr.2021.09.010